DOI: 10.26599/FSHW.2026.9251302

Contents lists available at SciOpen

Food Science and Human Wellness

journal homepage: https://www.sciopen.com/journal/2097-0765

China Food Publishing Co.

Lacticaseibacillus paracasei JY062 postbiotic ameliorates DSS-induced colitis in mice through the miR-6974-5p/IL-17A/MAPK/AP-1 axis

Jinfeng Guo [a], Yunlei Chai [a], Kaiqi Gao[a], Yilin Sun[a], Yue Su[a], Ying Zhao[a], Yu Zhang[a,*], Yujun Jiang[a,b,*]

[a] *Key Lab of Dairy Science, Ministry of Education, College of Food Science, Northeast Agricultural University, Harbin, Heilongjiang Province 150030, China*

[b] *Food Laboratory of Zhongyuan, Luohe, Henan Province 462300, China*

ABSTRACT: MicroRNAs (miRNAs) are key regulators of gene expression that play crucial roles in ulcerative colitis (UC) by regulating intestinal barrier function and modulating inflammatory signaling pathways. *Lacticaseibacillus paracasei* JY062 postbiotic (Pa JY062) has been shown to exert protective effects against colitis via regulating intestinal barrier function and mitigating inflammation; however, its underlying mechanisms involving the miRNA-mRNA axis remain unexplored. In this study, an integrated transcriptomic approach was employed to analyze the differential expression profiles of miRNAs and mRNAs in dextran sulfate sodium (DSS)-induced colitis mice treated with a high dose of Pa JY062. Initially, significantly differentially expressed miRNAs (DEM) were screened, followed by prediction of immune-related target genes for these miRNAs. Concurrently, significantly expressed gene mRNAs (DEG) were filtered from the transcriptomic data. Ultimately, based on the negative regulatory relationships between miRNAs and mRNAs, key regulatory pairs were identified: miR-6974-5p/IL-17A, miR-7094-1-5p/IL-17A, and miR-7013-3p/CCL19. In vitro validation using RAW264.7 cells demonstrated that miR-6974-5p attenuates inflammatory responses by directly targeting IL-17A, whereas neither miR-7094-1-5p nor miR-7013-3p significantly affected IL-17A or CCL19 expression under the same conditions. Additionally, dual-luciferase reporter assays confirmed that miR-6974-5p directly bound to the 3' untranslated region of IL-17A, thereby suppressing its expression. Furthermore, in vivo overexpression of miR-6974-5p via adeno-associated virus (AAV)-mediated delivery significantly alleviated colitis symptoms and pathological damage in mice, accompanied by marked inhibition of the protein expression of IL-17A, MAPK key indicators (p38, p-p38, JNK, p-JNK), and AP-1. Combined treatment with Pa JY062 and miR-6974-5p overexpression achieved the most pronounced protective effects, further supporting that Pa JY062 acts through upregulating this miRNA. Collectively, these results demonstrate that Pa JY062 ameliorates DSS-induced colitis by upregulating miR-6974-5p, which directly targets IL-17A and suppresses the downstream MAPK/AP-1 signaling pathway, revealing a novel miRNA-dependent mechanism that provides a scientific basis for developing functional foods and miRNA-targeted therapies for UC.

Keywords: *Lacticaseibacillus paracasei*; Postbiotic; miRNA; Ulcerative colitis; Inflammation

1. Introduction

***Corresponding author**
yujun_jiang@163.com; jessedevil@163.com;

Received 31 December 2025
Received in revised form 17 March 2026
Accepted 23 March 2026

MicroRNAs (miRNAs) are crucial regulators of gene expression that modulate target mRNA levels through base-pairing interactions [1]. These miRNAs influence ulcerative colitis (UC), a complex inflammatory bowel disease (IBD) [2], primarily by regulating intestinal barrier function, modulating inflammatory signaling, and maintaining gut microbiota homeostasis. Specifically, miR-24-3p, which is upregulated in active UC, promotes mucosal cell apoptosis and exacerbates inflammatory damage [3]. Members of the miR-200 family (miR-200a/b/c), along with miR-141, miR-429, and miR-27b, are downregulated in inflamed colonic tissues, a change linked to impaired epithelial barrier function via altered expression of their target genes (e.g., *ZEB2*, *RUNX1*) [4]. Additionally, miR-200b-3p can interact with bacteria to regulate microbiota composition, thereby contributing to intestinal barrier integrity and homeostasis [5].

Given the central role of miRNAs in UC, targeting miRNA-mRNA axis represents a promising therapeutic strategy. Postbiotics are defined as "preparations of inanimate microorganisms and/or their components that confer a health benefit on the host" [6]. Probiotic extracellular vesicles (EVs) are recognized as a type of postbiotic and have consequently garnered significant attention in UC research [7, 8]. Currently, research on postbiotic regulation of the miRNA-mRNA axis primarily focuses on probiotic EVs [9, 10], with limited exploration into milk-derived postbiotics directly targeting miRNA-mRNA interactions.

Pa JY062 is a novel food-derived postbiotic that significantly alleviates intestinal inflammation, restores disrupted intestinal barrier function, and modulates gut microbiota imbalance in vitro [11] and in DSS-induced mice [12]. However, the precise molecular mechanisms underlying miRNA-mRNA networks remain entirely unexplored. Hence, this study employs transcriptomic screening to identify differential miRNAs and mRNAs between DSS-treated mice and those receiving high-dose Pa JY062. Candidate miRNA-mRNA axes are then subjected to functional validation in vitro and in vivo. The aim is to identify and characterize a novel miRNA-mRNA axis as the core mechanism underlying Pa JY062's anti-colitis effect, thereby providing a theoretical basis for the application of milk-derived postbiotics in alleviating UC.

2. Materials and methods

2.1 Preparation and composition analysis of PaJY062 postbiotic and DSS-induced colitis model

Lacticaseibacillus paracasei JY062 was subcultured twice in MRS broth. The bacterial cells were harvested by centrifugation (10,000 × g, 5 min, 4 °C), washed twice with sterile PBS (pH 7.2), and resuspended in 10% skim milk containing 2% glucose. A 5% inoculum was incubated at 37°C for 16 h with shaking at 150 rpm. The fermented skim milk was heat-inactivated, pre-frozen at −80 °C for 24 h, and then freeze-dried for 36 h. The resulting powder was ground into a uniform sterile powder and stored at 4 °C, this powder was PaJY062 postbiotic. To confirm inactivation, the postbiotic suspension was plated on MRS agar and incubated at 37 °C for 48 h; no colony growth was observed, confirming sterility.

The composition of PaJY062 postbiotic was analyzed using UHPLC-MS/MS. The detailed methods and results are described in our previous study [12].

The animal protocol was approved by the Animal Ethics Committee of Northeast Agricultural University (NEAUEC20230422) and conducted in compliance with ARRIVE guidelines. Thirty 8-week-old male BALB/c mice (20±2 g) were purchased from Chengdu Dossy Experimental Animals Co., Ltd (Sichuan, China) and randomized into 3 groups (n=10/group): control (Ctrl, sterile water), DSS (3% DSS, MP Biomedicals, CA, USA), and high-dose Pa JY062 (HP, 3%

DSS + 800 mg/kg Pa JY062). Mice were acclimatized for 7 days (23±2 °C, 55±10% humidity, 12 h light/dark cycle). Colitis was induced with 3% DSS ad libitum (days 1–7) in all groups except Ctrl. During remission (days 8–14), Ctrl/DSS groups received 200 μL sterile water daily; HP group received 200 μL Pa JY062. On day 15, mice were euthanized with 10% chloral hydrate by intraperitoneal injection. To identify differentially expressed miRNAs and mRNAs between the HP and DSS groups, colon tissues were frozen at −80 °C for transcriptome sequencing. The sample size of n=3 per group was selected to balance animal welfare considerations with the need for biologically meaningful data.

2.2 microRNA sequencing and analysis

Total RNA was extracted from the colon tissues of mice (n=3) in the Ctrl group, DSS group, and HP group using RNAplus Reagent (TARAKA, Dalian, China) according to the manufacturer's instructions. RNA integrity was verified via Agilent 5300 Bioanalyzer (Agilent Technologies, CA, USA) and quantified with NanoDrop2000 (Thermo Fisher Scientific, MA, USA). High-quality samples ($OD_{260/280}$≥1.8-2.2, $OD_{260/230}$≥2.0, RQN ≥6.5, 28S:18S ≥1.0) proceeded to library construction [13].

To identify miRNAs dysregulated in DSS-induced colitis and restored by Pa JY062 treatment, we performed miRNA sequencing and differential expression analysis. miRNA sequencing libraries were constructed from 1 μg high-integrity RNA using QIAseq miRNA Library Kit (Qiagen, New York, USA), involving 5' or 3' adapter ligation, first-strand cDNA synthesis, PCR amplification (11-12 cycles), and size selection. Libraries (Qubit 4.0-quantified) were paired-end sequenced on NovaSeq X Plus (Illumina, CA, USA). Raw reads were processed with Fastx-Toolkit (http://hannonlab.cshl.edu/fastx_toolkit/, default parameters) to generate clean reads (3' adapter trimming, poly-N/low-quality base removal (phred < 20)). Collapsed 18-32 nt sequences were mapped to the reference genome for annotation. Known miRNAs were identified via miRbase 22.0. Unmapped reads were filtered against Rfam/Repbase (excluding non-miRNA RNAs), and unannotated reads underwent de novo prediction by miRDeep2. Expression was quantified as TPM; differential expression was analyzed via DESeq2 ($|\log_2FC| \geq 1$, FDR < 0.05) or DEGseq ($|\log_2FC| \geq 1$, FDR < 0.001). miRNA target prediction was performed using miRanda, TargetScan, and RNAhybrid to identify conserved binding sites, followed by Gene Ontology (GO) analysis for functional annotation.

To further refine the candidate miRNA set, differentially expressed miRNAs were filtered using the following four criteria: Criterion 1 required significant upregulation across DSS vs. Ctrl, HP vs. Ctrl, and DSS vs. HP comparisons; Criterion 2 required significant upregulation in DSS vs. Ctrl and DSS vs. HP but only non-significant upregulation in HP vs. Ctrl; Criterion 3 required significant downregulation across all three comparisons; Criterion 4 required significant downregulation in DSS vs. Ctrl and DSS vs. HP with non-significant downregulation in HP vs. Ctrl.

2.3 mRNA sequencing and analysis

To identify genes that are dysregulated in DSS-induced colitis and restored by Pa JY062 treatment, we performed mRNA sequencing and differential expression analysis. mRNA sequencing libraries were prepared from 1 μg total RNA using Illumina® Stranded mRNA Prep (poly(A) selection, fragmentation, cDNA synthesis, adapter ligation, 300-400 bp size selection) and amplified (10-15 cycles). Qubit 4.0 (Thermo Fisher Scientific, MA, USA) quantified libraries were sequenced on NovaSeq X Plus (PE150). Raw reads were processed with fastp (adapter trimming, quality control), mapped to the reference genome (HISAT2), and assembled via StringTie. Gene quantification (TPM) was done with RSEM.

Differential expression (DESeq2) defined DEGs as $|\log_2 FC| \geq 1$, FDR < 0.05. DEGs were functionally enriched (GO/KEGG; Goatools, SciPy; *Padj* < 0.05). To further refine the candidate gene set, differentially expressed genes were filtered using four criteria designed to capture genes consistently altered by DSS and reversed by Pa JY062 intervention. Differentially expressed genes were identified based on the following four criteria. Criterion 1: significant downregulation across DSS vs. Ctrl, HP vs. Ctrl, and DSS vs. HP comparisons. Criterion 2: significant downregulation in DSS vs. Ctrl and DSS vs. HP, with non-significant downregulation in HP vs. Ctrl. Criterion 3: significant upregulation across all three comparisons. Criterion 4: significant upregulation in DSS vs. Ctrl and DSS vs. HP, with non-significant upregulation in HP vs. Ctrl.

2.4 Interaction analysis of differentially expressed miRNA target genes and mRNA differentially expressed genes

To identify candidate miRNA-mRNA regulatory pairs, we performed integrated analysis of differentially expressed miRNAs and mRNAs. First, target genes of differentially expressed miRNAs were predicted using professional bioinformatics tools (e.g., miRanda, TargetScan) to generate potential target gene sets. These predicted target genes were then intersected with mRNA differentially expressed genes (identified via DESeq2) to screen for genes that were both miRNA targets and differentially expressed mRNAs—key candidates involved in miRNA-mRNA regulatory interactions. Functional enrichment analyses were performed on these intersecting genes: GO term enrichment (biological process, molecular function, cellular component) to explore functional characteristics, and Kyoto Encyclopedia of Genes and Genomes (KEGG) pathway enrichment to identify involved biological pathways. Significance was defined as $P < 0.05$. Additionally, a regulatory network was constructed to visualize interactions between differentially expressed miRNAs, their target genes (intersecting genes), and other related differentially expressed mRNAs. Combined with gene expression data, this network facilitated in-depth analysis of the coordinated miRNA-mRNA regulatory mechanisms in biological processes.

2.5 Culture and transfection of RAW264.7 cells

To validate the regulatory effects of candidate miRNAs on inflammatory responses, we performed transfection experiments in RAW264.7 cells. RAW264.7 cells were seeded in 12-well plates at 5×10^4 cells/well in high-glucose DMEM (10% FBS, 1% penicillin-streptomycin) and cultured for 24 h until 80% confluent. The supernatant was removed, and the cells were treated with 10 ng/mL LPS in medium for 12 h. After removing the supernatant, cells were gently washed 3 times with PBS, then 1 mL high-glucose DMEM (serum- and antibiotic-free) was added to eliminate interference from LPS, serum, and antibiotics on transfection reagents.

RAW264.7 cells were divided into nine transfection groups: blank control (Ctrl), mimics NC, inhibitor NC, miR-6974-5p mimics, miR-6974-5p inhibitor, miR-7094-1-5p mimics, miR-7094-1-5p inhibitor, miR-7013-3p mimics, and miR-7013-3p inhibitor (miRNA synthesis details in Table 1). Transfection was performed using the Xfect transfection reagent kit (TARAKA, Dalian, China), strictly according to the manufacturer's instructions. Briefly, miRNAs at a final concentration of 50 pmol were complexed with the transfection reagent. A 100 μL aliquot of the complex was added dropwise to each well. After gentle mixing, the cells were incubated for 4 h at 37 °C. The transfection medium was then replaced with 1 mL fresh culture medium, and cells were cultured for another 24 h. Each treatment was performed with three independent biological replicates (n=3) to collect sufficient cells for subsequent analyses.

Table 1. Specifications of chemically synthesized miRNAs for in vitro functional studies

miRNA name	Primer type	Sequence (5'→3')
mimics NC	Sense strand	UUUGUACUACACAAAAGUACUG
	Antisense strand	GUACUUUUGUGUAGUACAAAUU
inhibitor NC	Single strand	mCmAmGmUmAmCmUmUmUmUmGmUmGmUmAmGmUmAmCmAmAmA
miR-6974-5p mimics	Sense strand	GUGAGGCAGCAAGAGAUUGGGGGU
	Antisense strand	CCCCAAUCUCUUGCUGCCUCACUU
miR-6974-5p inhibitor	Single strand	mAmCmCmCmCmCmAmAmUmCmUmCmUmUmGmCmUmGmCmCmUmCmAmC
miR-7013-3p mimics	Sense strand	CCACACUUACUGUUGCCUCUUCCU
	Antisense strand	GAAGAGGCAACAGUAAGUGUGGUU
miR-7013-3p inhibitor	Single strand	mAmGmGmAmAmGmAmGmGmCmAmAmCmAmGmUmAmAmGmUmGmUmGmG
miR-7094-1-5p mimics	Sense strand	UCUGAAGAGGAUACAGGGUCUGA
	Antisense strand	AGACCCUGUAUCCUCUUCAGAUU
miR-7094-1-5p inhibitor	Single strand	mUmCmAmGmAmCmCmCmUmGmUmAmUmCmCmUmCmUmUmCmAmGmA

2.6 Real-time quantitative PCR to detect the expression changes of significantly different miRNAs and their target genes mRNA

To assess the regulatory effects of miRNAs on their target genes, total RNA was extracted from transfected cells using RNAiso Plus (TARAKA, Dalian, China) after 24 h transfection, and RNA concentration and purity were determined. Poly(A) tailing, cDNA synthesis, and real-time quantitative PCR (RT-qPCR) were performed following MiR-XTM miRNA First-Strand Synthesis and TB Green RT-qPCR kit (TARAKA, Dalian, China) protocols. U6 served as the internal reference for miRNA RT-qPCR, with miRNA expression calculated via the $2^{-\triangle\triangle Ct}$ method. For mRNA detection, total RNA was reverse-transcribed into cDNA, and GAPDH as the internal reference, target gene-specific primers (Table 2) were used for RT-qPCR to analyze miRNA-mediated regulation at the mRNA level.

Table 2. Primer Sequences for qPCR Detection of miRNAs and Target Genes

miRNA Name	Primer type	Sequence (5'→3')	Product length (bp)
miR-6974-5p	Forward	AACAATGTGAGGCAGCAAGAGAT	76
	Reverse	CAGTGCAGGGTCCGAGGT	
miR-7094-1-5p	Forward	CGACGCGATCTGAAGAGGATAC	77
	Reverse	CAGTGCAGGGTCCGAGGT	
miR-7013-3p	Forward	AACACGCCCACACTTACTGTTG	77
	Reverse	CAGTGCAGGGTCCGAGGT	
Il17a	Forward	TACCTCAACCGTTCCACGTC	119
	Reverse	TTTCCCTCCGCATTGACACA	
Ccl19	Forward	GGGGTGCTAATGATGCGGAA	137
	Reverse	CCTTAGTGTGGTGAACACAACA	

2.7 Effect of miRNA on inflammatory factors in RAW264.7 cells

To assess the effect of miRNA modulation on inflammatory cytokine secretion, culture supernatants from RAW264.7 cells were collected 24 hours post-transfection. Concentrations of inflammatory factors IL-17A and CCL19 were quantified using species-specific ELISA kits (Xinle Biotechnology, Shanghai, China) according to manufacturer protocols.

2.8 Western blot to detect the expression difference of target protein

To evaluate whether miRNA modulation alters the expression of target proteins, IL-17A protein levels in cell lysates were analyzed by western blot. Specifically, four hours post-transfection, the culture supernatant was aspirated. The cells

were then washed three times with PBS, followed by lysis and collection using cell lysis buffer (Beyotime, Shanghai, China) with 1%PMSF (Solarbio, Beijing, China), and protein concentration was determined using a BCA Protein Assay Kit (Solarbio, Beijing, China). Proteins (40 μg) were separated by 10% SDS-PAGE and transferred to PVDF membranes (0.45 μm). Membranes were blocked with 5% non-fat milk in TBST for 1 h at room temperature and incubated overnight at 4 °C with primary antibodies: rabbit anti-IL-17A (1:1000, bs-2140R, Bioss, China) and rabbit anti-GAPDH (1:5000, bs-10900R, Bioss, China) as an internal control. After washing with TBST, membranes were incubated with HRP-conjugated secondary antibodies (goat anti-rabbit IgG, 1:5000, bs-0295G-HRP, Bioss, China) for 1 h at room temperature. Protein bands were visualized using enhanced chemiluminescence (ECL) reagent and quantified via ImageJ software.

2.9 Dual luciferase reporter gene assay to evaluate the regulation of miRNA on target gene expression

To validate miRNA-mediated regulation of Il17a, a 192 bp fragment spanning the predicted miRNA binding site in the Il17a 3' untranslated region (UTR) was synthesized. The wild-type (WT) fragment was amplified using forward primer 5'-CTAGTTGTTTAAACGAGCTCGCTAGCACA

GAGACCCGCGGCTGACCCCTAAGAAA-3' and reverse primer 5'-GCCTGCAGGTCGAC

TCTAGACTCGAGAACACGAAGCAGTTTGGGACCCCTTTACA-3', which introduced NheI and XhoI restriction sites at the ends. The mutant (MT) fragment, containing disrupted miRNA binding motifs, was generated by site-directed mutagenesis. Both fragments were double-digested with NheI and XhoI (NEB, USA) and cloned into the pmirGLO vector (Promega, WI, USA) downstream of the firefly luciferase gene. Ligation was performed using T4 DNA ligase (Fermentas, USA), and the recombinant plasmids were transformed into E. coli TOP10 competent cells. Positive clones were identified by colony PCR and confirmed by DNA sequencing (Wuhan Genecreate Biological Engineering Co., Ltd., China). The successfully constructed WT and MT plasmids were extracted and quantified using a NanoDrop 2000 spectrophotometer (Thermo Fisher Scientific, USA). HEK293T cells seeded in 24-well plates (60–70% confluency, DMEM + 10% FBS) 24 h prior were transfected with mixtures of 200 ng WT/MT plasmid, 50 nM mimics/NC, and 4 μL Lipofectamine 2000 (Invitrogen, California, USA) in serum-free DMEM (15 min incubation, 500 μL final volume). After 4 h at 37 °C, medium was replaced with 1 mL complete DMEM for 48 h. Cells were lysed with 200 μL lysis buffer, incubated on ice for 5 min, and centrifuged at 10,000 rpm for 5 min. Supernatant (20 μL) was transferred to 96-well plates, and luciferase activity was measured sequentially with Firefly (350–700 nm, 1 s) and Renilla reagents. Firefly signals were normalized to Renilla (RLU ratio), with fold changes relative to NC. Data are from three independent experiments (n=3), each performed in triplicate.

2.10 Construction and concentration of adeno-associated virus

To functionally validate whether the candidate miR-6974-5p identified from transcriptomic screening is sufficient to alleviate colitis, we constructed a recombinant adeno-associated virus (AAV) vector. miR-6974-5p (sequence: GUGAGGCAGCAAGAGAUUGGGGGU) was cloned into the pAV-CD68-GFP-miR30-shRNA adeno-associated virus (AAV) vector to generate the recombinant plasmid. This vector employs a recombinational cloning strategy based on BpiI (BbsI) restriction sites (WZ Biosciences, Inc, Shandong, China). The resulting plasmid was co-transfected with the Ad Helper Vector and pAAVrep/cap Vector into HEK293T cells for viral packaging. After 72 h of transfection, culture supernatants were filtered through 0.45 μm membranes and cell pellets were separately harvested. Viral particles in

supernatants were precipitated using PEG8000. The virus was further purified via iodixanol-based density gradient centrifugation to enhance titer, and virus purity was determined by SDS-PAGE. The final titers were quantified by qPCR, the standard protocol curve (copy count) and CT values can be defined based on the measured CT value (period threshold) and the standard product concentration of the standard product. AAV viral titer (vg/mL) was calculated as:

$$\text{Titer (vg/mL)} = \frac{qPCR\ derived\ copy\ number \times dilution\ factor}{template\ volume\ (mL)}$$

2.11 AAV2-mediated miRNA-6974-5p overexpression for therapeutic evaluation in mice

To extend our in vitro findings to an in vivo setting and to determine whether miR-6974-5p serves as a key downstream effector of Pa JY062, we performed AAV-mediated miR-6974-5p overexpression in DSS-induced colitis mice, with or without Pa JY062 treatment. Forty 4-week-old SPF female BALB/c mice (15-17 g) were purchased from Beijing Weitonglihua Experimental Animal Technology Co., Ltd. They were housed 5 per cage for a 3-day acclimatization to the environment. All animal procedures were approved by the Institutional Animal Care and Use Committee of Northeast Agricultural University (approval number: NEAUEC20230422) and conducted in accordance with ARRIVE guidelines. Mice were randomized into four groups (n = 10 per group): (1) Ctrl group received standard diet throughout, and was administered sterile saline (200 μL/day) by oral gavage during the final 7 days of the experimental period. (2) AAV2-miR-scramble group received intrarectal administration of pAV-CD68-GFP-miR30-shRNA-miR-scramble vectors (1×10^{11} vg/mL) after acclimatization, followed by a 21-day maintenance period, with 3% DSS provided in drinking water during the final 7 days. During this DSS treatment period, the mice also received sterile saline (200 μL/day) by oral gavage. (3) AAV2-miR-6974-5p group received identical intrarectal administration with pAV-CD68-GFP-miR30-shRNA-miRNA-6974-5p vectors, together with oral gavage of sterile saline (200 μL/day) during the final 7 days of DSS treatment. (4) Pa JY062 + AAV2-miR-6974-5p group received the same intrarectal administration of AAV2-miR-6974-5p vectors as group 3, combined with oral gavage of Pa JY062 (800 mg/kg body weight, 200 μL/mouse) during the final 7 days of DSS treatment. Mice scheduled for enema administration (all groups except the control) were fasted for 12 h with water deprivation prior to anesthesia. Following anesthesia, animals received 300 μL of 20 mM N-acetyl-L-cysteine (Sigma-Aldrich, MO, USA) and 2.5 mg/kg pilocarpine (Sigma-Aldrich, MO, USA) to clear intestinal mucus, then underwent AAV enema. Daily measurements included body weight recording. During DSS exposure, fecal consistency, occult blood levels, food intake, and water consumption were monitored daily per cage. After 7 days of DSS treatment, mice were euthanized under anesthesia. Colon tissues were harvested for length measurement, with segments fixed in 4% paraformaldehyde for subsequent H&E staining and immunohistochemistry, while parallel segments underwent western blot analysis and ELISA quantification.

2.12 Hematoxylin and eosin (H&E) staining of colonic tissues in mice

To evaluate the protective effects of miR-6974-5p and Pa JY062 on colonic histopathology, H&E staining was performed, and histological scores were assessed. Colonic tissues were fixed in 4% paraformaldehyde at 4 °C for 24 h, dehydrated through graded ethanol (70-100%), cleared in xylene, embedded in paraffin, sectioned at 4 μm, mounted on poly-L-lysine-coated slides, and baked at 60 °C for 2 h. For H&E staining, sections were deparaffinized, rehydrated, stained with Harris hematoxylin (Sigma-Aldrich, Missouri, USA) for 5 min, rinsed, differentiated in 1% hydrochloric acid-ethanol, re-blued in 0.5% ammonia water, counterstained with 0.5% eosin Y (Sigma-Aldrich, Missouri, USA) for 2 min, dehydrated,

cleared, and mounted with DPX (Sigma-Aldrich, Missouri, USA). Sections were imaged at 200×, and histopathological scoring was performed blindly by two researchers (Wang et al., 2021).

2.13 IL-17A detection in mice

To evaluate the effect of miR-6974-5p and Pa JY062 on colonic inflammation, IL-17A levels in colon tissues were quantified by ELISA. Frozen colon tissues (50 mg) were pulverized in liquid nitrogen using a pre-cooled mortar. The powder was homogenized in 10 volumes of ice-cold PBS containing PMSF (1:10, w/v) and centrifuged at 12,000 × g for 15 min at 4 °C. The supernatant was collected, and total protein concentration was determined by BCA assay. All samples were normalized to 3 mg/mL with PBS for subsequent analysis. Colon inflammatory factor IL-17A was measured by ELISA kits (Xinle Biotechnology, Shanghai, China) according to manufacturer protocols. All assays were performed in triplicate.

2.14 Effect of miRNA on key pathway proteins in Pa JY062 postbiotic mediated amelioration of DSS-induced colitis in mice

To determine whether miR-6974-5p overexpression and combined Pa JY062 treatment suppress the IL-17A/MAPK/AP-1 signaling axis in vivo, protein expression levels of IL-17A, p38, p-p38, JNK, p-JNK and AP-1 in colon tissues were analyzed by Western blot. Colon tissue protein lysates were prepared using the same liquid nitrogen grinding method described for ELISA. Proteins (40 μg per lane) were separated by SDS-PAGE and transferred to PVDF membranes. After blocking, the membranes were incubated overnight at 4 °C with the following primary antibodies diluted in 3% BSA: mouse anti-GAPDH (Proteintech, 60004-1-Ig, 1:10,000), mouse anti-IL-17A (Bioss, BS-1183R, 1:2,000), rabbit anti-p38 (HUABIO, ET1702-65, 1:5,000), rabbit anti-p-p38 (YOUPIN, YP-Ab-14472, 1:1000), mouse anti- JNK (Proteintech, 66210-1-Ig, 1:2000), rabbit anti-p-JNK (ABclonal, AP0631, 1:1000) and rabbit anti-AP-1 (HUABIO, ER62677, 1:2,000). Following washes, membranes were incubated with corresponding HRP-conjugated secondary antibodies diluted in 5% non-fat milk: goat anti-rabbit (Seracare, 5220-0336, 1:50,000) or goat anti-mouse (Seracare, 5220-0341, 1:50,000) for 1 h at room temperature. Protein bands were visualized using ECL substrate and quantified by densitometry. Relative expression levels of IL-17A, p38, p-p38, JNK, p-JNK and AP-1 were compared across the Ctrl, AAV2-miR-scramble, AAV2-miR-6974-5p, and Pa JY062 + AAV2-miR-6974-5p groups to analyze the regulatory mechanism of miR-6974-5p in 3% DSS-induced murine colitis.

2.15 Statistical analysis

All data are presented as mean ± standard error (SEM). Normality was assessed using the Shapiro-Wilk test, and homogeneity of variances was assessed using Levene's test. For comparisons among multiple groups, one-way analysis of variance (ANOVA) followed by Duncan's post hoc test was performed. For comparisons between two groups, Student's t-test was used (SPSS 26.0). A $p<0.05$ was considered statistically significant, and different lowercase letters indicate significant differences between groups.

For transcriptome sequencing data, differential expression was analyzed using DESeq2, with a false discovery rate (FDR) < 0.05 applied to correct for multiple comparisons. All experiments were performed with three independent biological replicates, each with three technical replicates.

3. Results

3.1 Sequencing data quality control

Quality control procedures for both miRNA and mRNA sequencing datasets included adapter trimming, removal of low-quality bases (Q<20), elimination of reads containing ambiguous bases (N), and size selection (miRNA: 18–32 nt). All samples exhibited optimal metrics: GC content≈50%, Q20 bases >99% (miRNA) and >98.36% (mRNA), and Q30 bases >96% (miRNA) and >95.14% (mRNA), which significantly exceeded standard thresholds (Q20>85%, Q30>80%). Specifically, miRNA sequencing yielded 6.13-6.20 million usable reads per sample (e.g., Ctrl-1: 6,130,302 from 6,198,745 clean reads), while mRNA sequencing generated 57.93 Gb clean data across 9 samples (≥6.04 Gb/sample), with >40.78 million clean reads per sample. Comprehensive quality metrics are detailed in Tables 3-4. These data indicate high sequencing quality, which was adequate for all downstream analyses.

Table 3. Quality Metrics of miRNA-Seq Data (Post-QC)

Sample	Clean reads	Error rate (%)	Q20(%)	Q30(%)	GC content (%)	Useful reads
Ctrl-1	6198745	0.0115	99.24	96.86	51.25	6130302
Ctrl-2	9707470	0.0117	99.05	96.49	49.46	9435027
Ctrl-3	8774308	0.0111	99.48	97.48	47.4	8658641
DSS-1	8496203	0.0112	99.38	97.34	49.12	8249264
DSS-2	7659738	0.0114	99.31	97.04	48.74	7395272
DSS-3	9543809	0.0119	98.95	96	49.18	9118468
HP-1	9371753	0.0114	99.32	97.04	48.23	9194549
HP-2	8887997	0.0112	99.38	97.3	46.38	8738977
HP-3	8838181	0.0112	99.42	97.37	47.91	8564458

Table 4. Quality Metrics of mRNA-Seq Data (Post-QC)

Sample	Raw reads	Clean reads	Error rate (%)	Q20(%)	Q30(%)	GC content (%)
Ctrl-1	44851912	44327390	0.0124	98.45	95.35	51.02
Ctrl-2	44676158	44198014	0.0122	98.55	95.68	50.6
Ctrl-3	41375616	40906844	0.0123	98.47	95.47	51.06
DSS-1	44960852	44356272	0.0123	98.48	95.49	50.8
DSS-2	43821548	43240384	0.0124	98.43	95.31	50.26
DSS-3	45622248	45115744	0.0124	98.43	95.35	50.17
HP-1	41274482	40781908	0.0125	98.36	95.14	50.77
HP-2	43381022	42844248	0.0125	98.39	95.25	51.87
HP-3	40869594	40354612	0.0124	98.43	95.43	51.52

3.2 Differential expression analysis of miRNA in colon tissue

To identify miRNA-mRNA regulatory networks involved in colonic inflammation in mice, we performed miRNA sequencing on colonic tissues from Control group (Ctrl), DSS group, and High-dose Pa JY062 (HP) groups (n=3). miRNA sequencing of colonic tissues revealed 58 differentially expressed miRNAs (DEMs) in DSS versus Control groups (38 upregulated, 20 downregulated; $|\log_2 FC| \geq 1$, $p < 0.05$), 35 DEMs in high-dose Pa JY062 (HP) versus Control (27 upregulated, 8 downregulated), and 40 DEMs in HP versus DSS (15 upregulated, 25 downregulated) (Fig. 1A). By applying four stringent criteria, 14 key DEMs were identified, of which three miRNAs met Criterion 1: miR-146b-5p, miR-155-5p and miR-135b-5p. Six miRNAs met Criterion 2: miR-3964, miR-106a-5p, miR-142a-3p, miR-802-3p, miR-31-5p, and miR-142a-5p. One miRNA met Criterion 3: miR-6974-5p. Four miRNAs met Criterion 4: miR-375-3p, miR-7094-1-5p, miR-7013-3p, and miR-6538 (Table 5).

Table 5. Differentially Expressed miRNAs Satisfying Four Screening Criteria

miRNA name	DSS vs Ctrl	HP vs Ctrl	DSS vs HP	Sum
miR-146b-5p	yes|up	yes|up	yes|up	3
miR-155-5p	yes|up	yes|up	yes|up	3
miR-135b-5p	yes|up	yes|up	yes|up	3
miR-6974-5p	yes|down	yes|down	yes|down	3
miR-375-3p	yes|down	no|down	yes|down	2
miR-7013-3p	yes|down	no|down	yes|down	2
miR-7094-1-5p	yes|down	no|down	yes|down	2
miR-31-5p	yes|up	no|up	yes|up	2
miR-106a-5p	yes|up	no|up	yes|up	2
miR-142a-3p	yes|up	no|up	yes|up	2
miR-142a-5p	yes|up	no|up	yes|up	2
miR-802-3p	yes|up	no|up	yes|up	2
miR-3964	yes|up	no|up	yes|up	2
miR-6538	yes|down	no|down	yes|down	2

Note: (1) Significance: yes ($P < 0.05$); no ($P > 0.05$). (2) Expression: up (upregulated); down (downregulated). (3) Sum: Total differentially expressed genes in three groups.

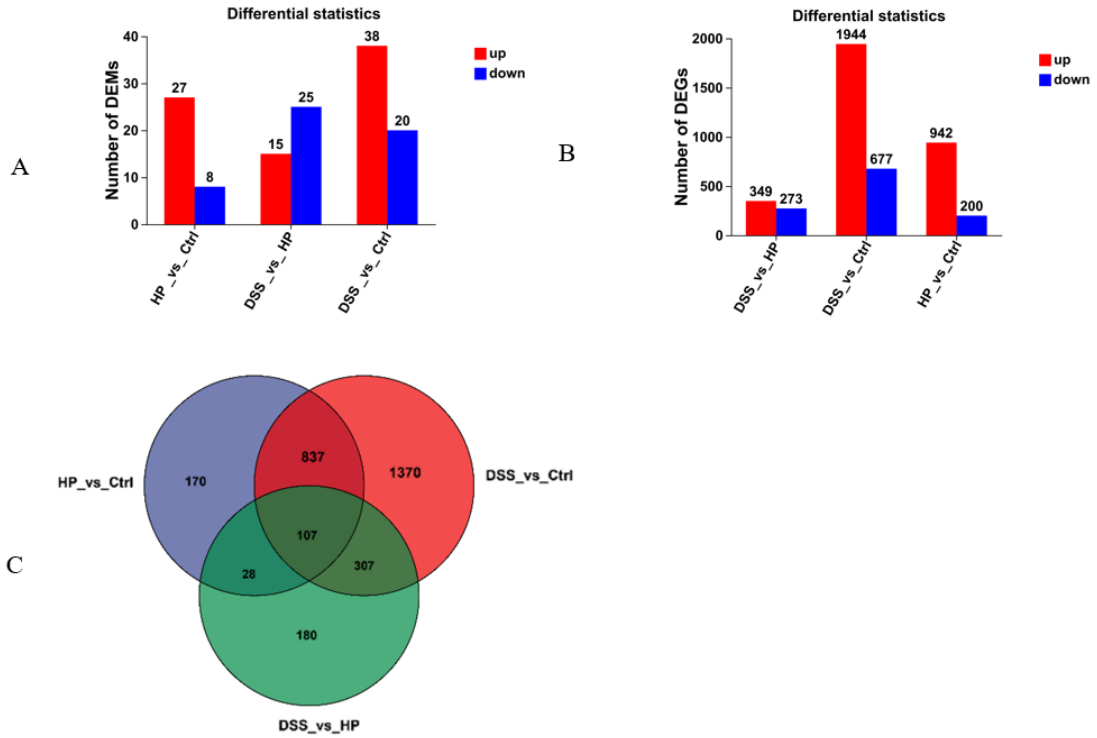


Fig.1. Landscape of Differential miRNA and mRNA Expression in Colitis. **(A)** Distribution of differentially expressed miRNAs (DEMs). **(B)** Distribution of differentially expressed genes (DEGs). **(C)** Overlap of DEG sets among groups, visualized by a Venn diagram. Upregulated and downregulated species are indicated in red and blue, respectively. Ctrl (healthy control), DSS (3% DSS treatment with natural recovery), and HP (3% DSS treatment with high-dose *Lacticaseibacillus paracasei* JY062 postbiotic (Pa JY062, 800 mg/kg) groups. All data represent mean ± SEM from three biological replicates (n=3).

3.3 miRNA target gene prediction

miRNAs function through post-transcriptional regulation of target genes. Using miRanda, TargetScan and RNAhybrid, we predicted targets of differentially expressed miRNAs and identified multiple immune-related molecules, consistent with UC's autoimmune pathology. The complete list of key predicted target genes for each miRNA is provided in Supplementary

Table S1- S14. Key predictions included (Table 6): IL-17A, a pro-inflammatory cytokine central to colitis pathogenesis, as a target of both miR-6974-5p and miR-7094-1-5p; CCL19, a chemokine involved in T cell recruitment to inflamed intestines, as a target of miR-7013-3p; Il6ra of miR-155-5p, a subunit crucial in inflammation and Th17 differentiation; Bach2 and Icos of miR-31-5p, regulating T cell function and activation; Braf and Klf4 of miR-146b-5p, involved in MAPK signaling and macrophage polarization; Ccr9 of miR-142a-3p, mediating gut lymphocyte homing. miR-802-3p targeted both IL-10 and IL-1α, which are key anti-inflammatory and pro-inflammatory cytokines, respectively.

Table 6. The key predicted target genes of miRNAs involved in immune regulation

miRNA name	target gene id	target gene name	target gene description
miR-155-5p	ENSMUSG00000027947	*Il6ra*	interleukin 6 receptor, alpha
miR-31-5p	ENSMUSG00000040270	*Bach2*	BTB and CNC homology, basic leucine zipper transcription factor 2
miR-31-5p	ENSMUSG00000026009	*Icos*	inducible T cell co-stimulator
miR-146b-5p	ENSMUSG00000002413	*Braf*	Braf transforming gene
miR-146b-5p	ENSMUSG00000003032	*Klf4*	Kruppel-like transcription factor 4 (gut)
miR-142a-3p	ENSMUSG00000029530	*Ccr9*	chemokine (C-C motif) receptor 9
miR-802-3p	ENSMUSG00000016529	*Il10*	interleukin 10
miR-802-3p	ENSMUSG00000027399	*Il1a*	interleukin 1 alpha
miR-6974-5p	ENSMUSG00000025929	*Il17a*	interleukin 17A
miR-7094-1-5p	ENSMUSG00000025929	*Il17a*	interleukin 17A

3.4 Differential expression analysis of mRNA in colon tissue

Differential expression analysis was performed using DESeq2 with a threshold of $|\log_2 FC| \geq 1$ and $P < 0.05$. DSS treatment markedly perturbed the colonic transcriptome, with the DSS vs Ctrl group showing 2,621 DEGs (1,944 upregulated, 677 downregulated). Intervention with Pa JY062 substantially attenuated this effect, as evidenced by 1,142 DEGs in the HP vs Ctrl group (942 upregulated, 200 downregulated). The DSS vs HP comparison, critical for elucidating the protective effect of Pa JY062, identified 622 DEGs (349 upregulated, 273 downregulated, Fig. 1B). Venn analysis further delineated the overlap among DEG sets. Specifically, 944 DEGs were shared between HP vs Ctrl and DSS vs Ctrl groups; 414 between DSS vs Ctrl and DSS vs HP groups; 135 between HP vs Ctrl and DSS vs HP groups, and 107 DEGs were common to all three comparisons (Fig. 1C).

3.5 Functional analysis of differentially expressed genes

Functional annotation of differentially expressed genes using GO, KEGG, and Reactome databases revealed their predominant involvement in immune-related processes, consistent with the autoimmune nature of UC. GO analysis highlighted enrichment in response to stimulus, biological regulation, cellular processes, and immune system processes (Fig. 2A). KEGG annotation showed highest enrichment in viral infections, followed by cancer, bacterial infections, and immune diseases (Fig. 2B). Reactome analysis identified significant enrichment in immune system, signal transduction, and metabolic pathways (Fig. 2C).

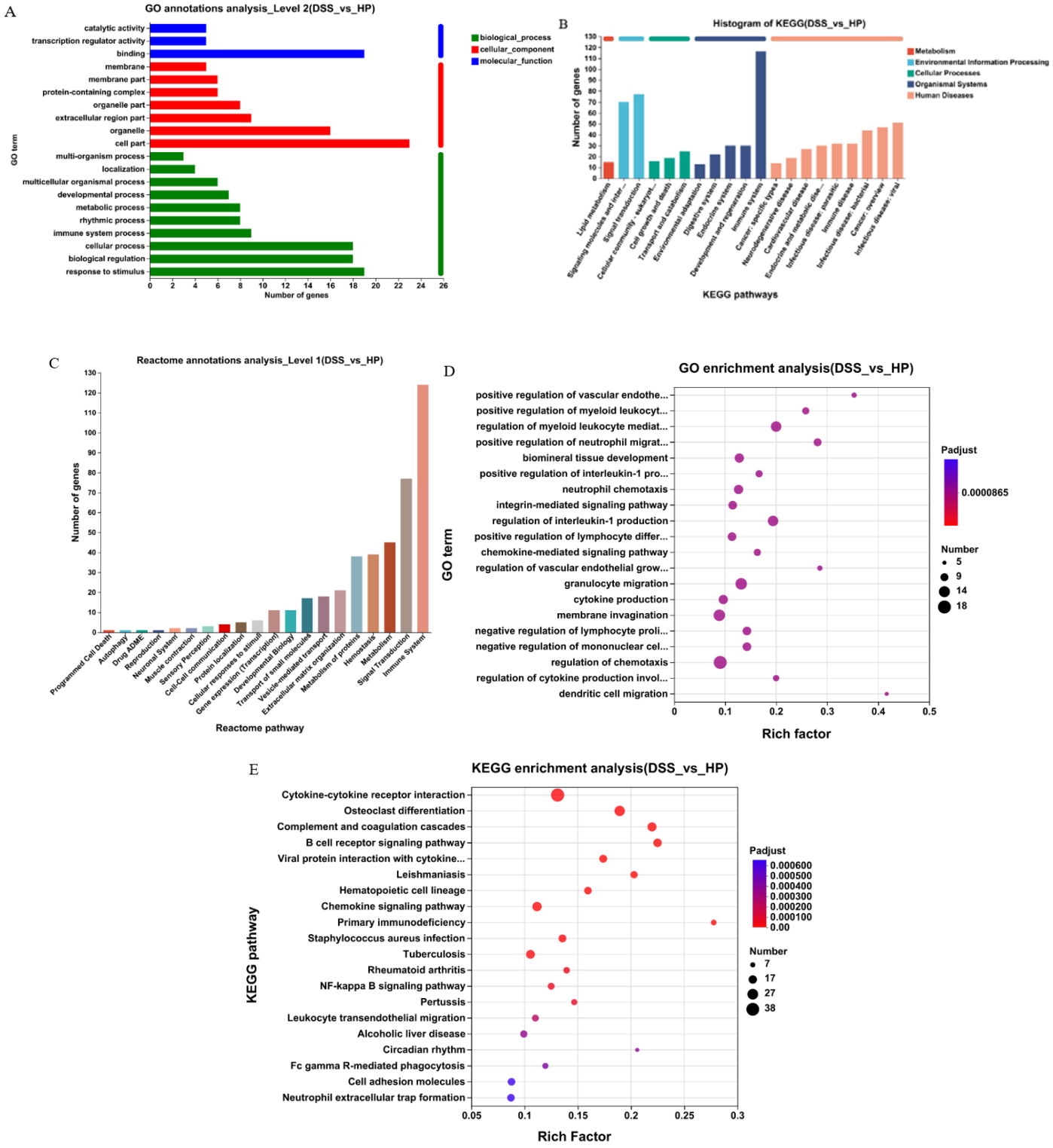


Fig.2. Functional annotation and enrichment analysis of differentially expressed genes (DEGs) in DSS _vs_HP. **(A–C)** Bar plots of functional annotation based on **(A)** Gene Ontology (GO), **(B)** KEGG, and **(C)** Reactome databases. **(D)** GO and **(E)** KEGG enrichment analysis bubble plots. Bar length and bubble size represent the number of enriched DEGs, with longer bars or larger bubbles indicating a greater number of genes. DSS: 3% DSS treatment with natural recovery; HP: 3% DSS treatment with high-dose Pa JY062 postbiotic (800 mg/kg). Data are presented as mean ± SEM from three biological replicates (n = 3).

Further enrichment analysis identified key immune pathways altered between DSS and treatment groups. GO analysis revealed significant differences in genes regulating chemotaxis (18 genes), membrane invagination (15 genes), granulocyte migration (15 genes), interleukin-1 production (13 genes), and myeloid leukocyte immune regulation (13 genes) (Fig. 2D). KEGG analysis showed the cytokine-cytokine receptor interaction pathway was most significantly enriched with 38 genes

(Fig. 2E). Among these, *Il17a* exhibited the most pronounced differential expression, with significant upregulation in DSS vs Ctrl ($log_2FC=8.40$, $P < 0.05$) and downregulation in DSS vs HP ($log_2FC=-2.98$, $P < 0.0001$). *Ccl19* showed the second highest differential expression (DSS vs Ctrl: $log_2FC=6.11$, $P < 0.0001$; DSS vs HP: $log_2FC=-1.75$, $P < 0.0001$, Table 7). Both *Il17a* and *Ccl19* were therefore selected for further investigation, with *Il17a* participating in the IL-17 signaling pathway involving MAPK and AP-1 activation (Fig. 3A), and *Ccl19* functioning within the chemokine signaling pathway (Fig. 3B).

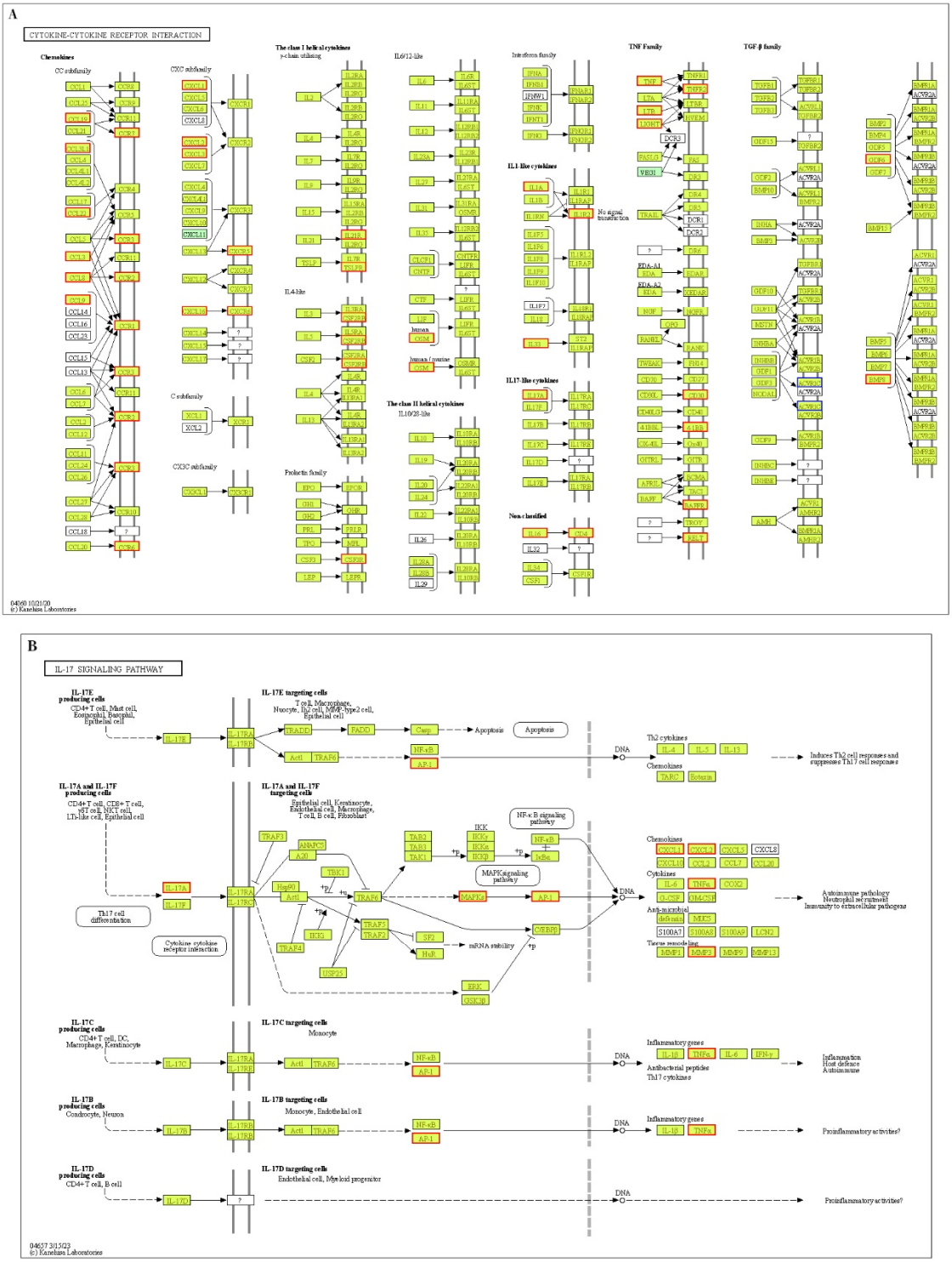


Fig.3. KEGG-based pathway analysis of key inflammatory signaling in DSS _vs_ HP. **(A)** Cytokine-cytokine receptor interaction pathway. **(B)** IL-17 signaling pathway. Red boxes highlight upregulated components; solid arrows indicate direct regulation, and dashed arrows indicate indirect interactions. DSS: 3% DSS treatment with natural recovery; HP: 3% DSS treatment with high-dose Pa JY062 postbiotic (800 mg/kg).

Table 7. The key significantly enriched differentially expressed genes in the cytokine-cytokine receptor interaction pathway

gene name	HP_ vs _Ctrl			DSS_ vs_ Ctrl			DSS _vs_ HP		
	regulate	log2fc	p<0.05	regulate	log2fc	*p*<0.05	regulate	log2fc	*p*<0.05
Il17a	up	5.41	yes	up	8.40	yes	up	2.98	yes
Tnfrsf9	up	2.61	yes	up	3.77	yes	up	1.15	yes
Il21r	up	1.68	yes	up	2.80	yes	up	1.10	yes
Ccr2	up	1.84	yes	up	2.91	yes	up	1.05	yes
Ccl19	up	4.35	yes	up	6.11	yes	up	1.75	yes

3.6 miRNA-mRNA interaction analysis

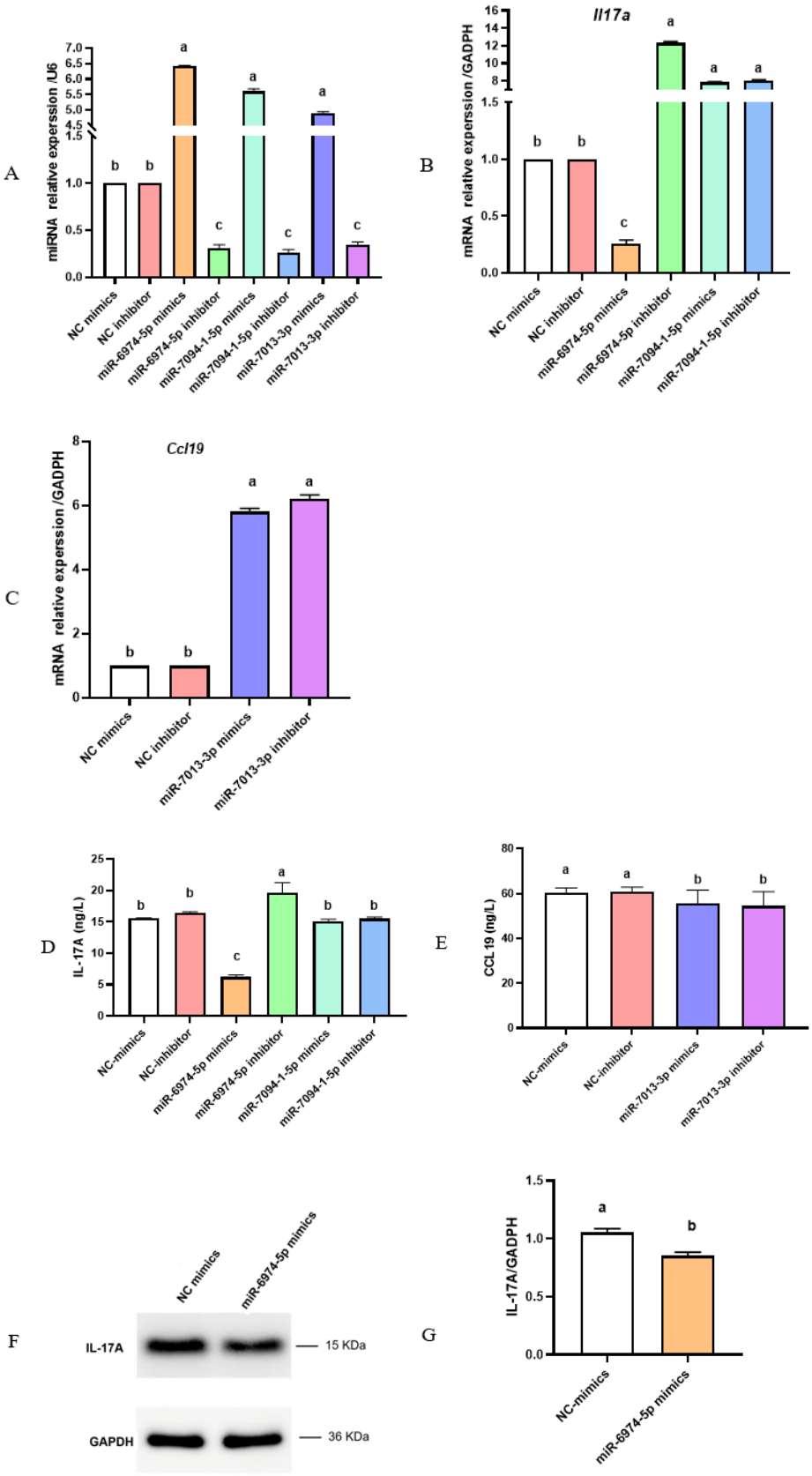
Integrated analysis of miRNA-mRNA interactions identified three candidate regulatory pairs with significant negative expression correlations (Table 8). *Il17a* was predicted as a common target of both miR-6974-5p and miR-7094-1-5p, while *Ccl19* was identified as a potential target of miR-7013-3p. In the DSS-induced colitis model, *Il17a* and *Ccl19* mRNA expression were significantly upregulated, while all three miRNAs showed corresponding downregulation. Following HP treatment, both miR-6974-5p expression and *Il17a* levels showed substantial recovery, whereas miR-7013-3p expression and its target *Ccl19* exhibited only partial normalization. These results suggest miR-6974-5p may play a particularly important role in the therapeutic mechanism of HP intervention.

Table 8. Candidate target genes exhibiting negative regulatory relationships with key miRNAs in the cytokine-cytokine receptor interaction pathway

Genes	DSS vs Ctrl	HP vs Ctrl	DSS vs HP	miRNA	DSS vs Ctrl	HP vs Ctrl	DSS vs HP
Il17a	yes|up	yes|up	yes|up	miR-6974-5p	yes|down	yes|down	yes|down
				miR-7094-1-5p	yes|down	no|down	yes|down
Ccl19	yes|up	yes|up	yes|up	miR-7013-3p	yes|down	no|down	yes|down

3.7 Overexpression and inhibition of miRNA affected the expression of miRNA and its target genes in RAW264.7 cells

Transfection efficiency and functional screening of candidate miRNAs in RAW264.7 cells were assessed by RT-qPCR. miR-6974-5p expression increased 6.4-fold with mimics and decreased to 0.31-fold with inhibitor relative to respective controls ($P < 0.05$). Similar trends were observed for miR-7094-1-5p (5.6-fold up, 0.26-fold down) and miR-7013-3p (4.9-fold up, 0.35-fold down) ($P < 0.05$), confirming effective miRNA modulation (Fig. 4A). Functionally, only miR-6974-5p significantly regulated its predicted target: its overexpression or inhibition markedly altered *Il17a* mRNA levels ($P < 0.05$, Fig. 4B). In contrast, neither miR-7094-1-5p nor miR-7013-3p significantly affected *Il17a* or *Ccl19* expression under these conditions ($P > 0.05$, Fig. 4C), suggesting their regulatory roles may be context-dependent and require further validation.


A
miRNA relative expression /U6
NC mimics
NC inhibitor
miR-6974-5p mimics
miR-6974-5p inhibitor
miR-7094-1-5p mimics
miR-7094-1-5p inhibitor
miR-7013-3p mimics
miR-7013-3p inhibitor
B
Il17a
mRNA relative expression /GADPH
C
Ccl19
D
IL-17A (ng/L)
NC-mimics
NC-inhibitor
E
CCL19 (ng/L)
F
IL-17A
GAPDH
15 KDa
36 KDa
G
IL-17A/GADPH

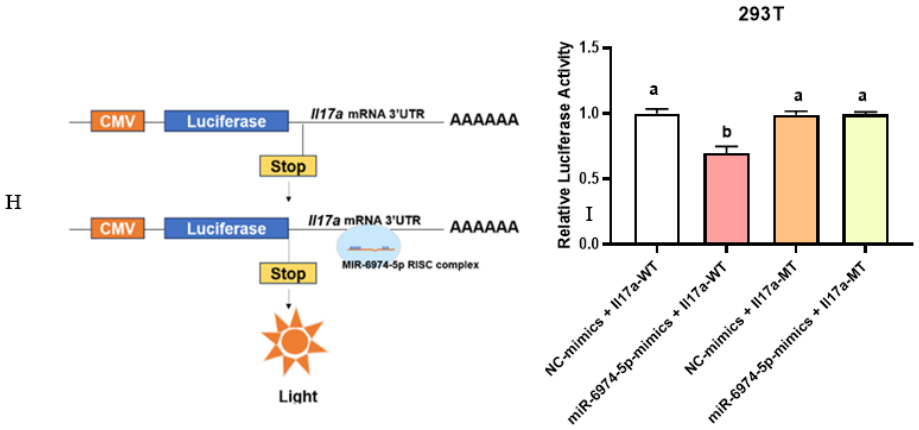


Fig.4. Functional validation of key miRNA–mRNA regulatory pairs in cellular models. **(A–G)** Analysis in RAW264.7 macrophages: **(A)** Relative expression of miRNAs after transfection. **(B)** *Il17a* and **(C)** *Ccl19* mRNA levels upon miRNA perturbation. **(D)** IL-17A secretion following overexpression or knockdown of miR-6974-5p and miR-7094-1-5p. **(E)** CCL19 secretion after modulation of miR-7013-3p expression. **(F)** Western blot and **(G)** quantification of IL-17A protein after miR-6974-5p overexpression**. (H–I)** Analysis in HEK293T cells: **(H)** Schematic of miR-6974-5p binding site on *Il17a* 3'UTR. **(I)** Relative luciferase activity of wild-type (WT) and mutant (MT) reporters. Mimics: overexpression; inhibitor: knockdown. U6 and *GAPDH* served as internal controls. Data are from three biological replicates (mean ± SEM).

3.8 Effects of differentially expressed miRNAs on inflammatory cytokines IL-17A and CCL19 in RAW264.7 cells

To experimentally validate whether miR-6974-5p and miR-7094-1-5p regulated their target IL-17A, and whether miR-7013-3p regulated CCL19, we measured IL-17A and CCL19 secretion in RAW264.7 cells. Overexpression of miR-6974-5p (via mimics) significantly suppressed IL-17A secretion, while its knockdown (via inhibitor) markedly enhanced secretion compared to control (Ctrl) ($P < 0.05$). In contrast, knockdown of miR-7094-1-5p did not affect IL-17A secretion (Fig. 4D). These results demonstrate that miR-6974-5p targets and regulates IL-17A expression. The difference in CCL19 secretion between miR-7013-3p overexpression and knockdown was not statistically significant, although both treatments resulted in a decreasing trend (Fig. 4E). This suggests that miR-7013-3p does not directly regulate CCL19 in this system. The observed reduction may have stemmed from indirect feedback mechanisms involving compensatory regulation of other factors. Collectively, these findings demonstrate that miR-6974-5p attenuates inflammatory responses in RAW264.7 cells by directly targeting IL-17A.

Western blot results aligned with mRNA findings: miR-6974-5p mimic downregulated IL-17A protein expression by 0.2-fold versus mimic NC ($P < 0.001$; Fig. 4F-G). Together, these data confirm that miR-6974-5p specifically regulates IL-17A at both transcriptional and translational levels, whereas miR-7094-1-5p and miR-7013-3p do not exhibit detectable regulatory effects on their predicted targets under these experimental conditions.

3.9 Dual-luciferase assays confirmed direct targeting of IL-17A 3'UTR by miR-6974-5p

To validate the direct interaction between miR-6974-5p and the 3'UTR of *Il17a*, dual-luciferase reporter assays were performed in HEK293T cells (Fig. 4H-I). Cells co-transfected with miR-6974-5p mimics and the wild-type *Il17a* 3'UTR reporter plasmid (*Il17a*-WT) showed a 0.42-fold reduction in relative luciferase activity compared to the NC mimics + *Il17a*-WT group ($P < 0.05$). In contrast, no significant difference was observed in relative luciferase activity between the miR-6974-5p mimics + *Il17a*-MT (mutant 3'UTR) group and the NC mimics + *Il17a*-MT group ($P > 0.05$; Fig. 4I). These results confirm that miR-6974-5p directly binds to the 3'UTR of *Il17a*, thereby suppressing translation of the reporter gene.

Collectively, our data demonstrate that miR-6974-5p can directly target and regulate *Il17a* expression, supporting its potential role in alleviating UC through modulation of *Il17a*-mediated inflammatory responses.

3.10 Constructed successfully of pAV-CD68-GFP-miR30-shRNA-miRNA-6974-5p vectors

To investigate the therapeutic potential of miR-6974-5p in vivo, we constructed a recombinant adeno-associated virus (AAV) vector by cloning miR-6974-5p into the pAV-CD68-miR30-shRNA backbone. The resulting plasmid, along with helper and rep/cap vectors, was transfected into HEK293T cells for viral packaging. At 72 hours post-transfection, cytopathic effects were observed (Fig. 5A), and strong GFP expression confirmed successful transduction (Fig. 5B).

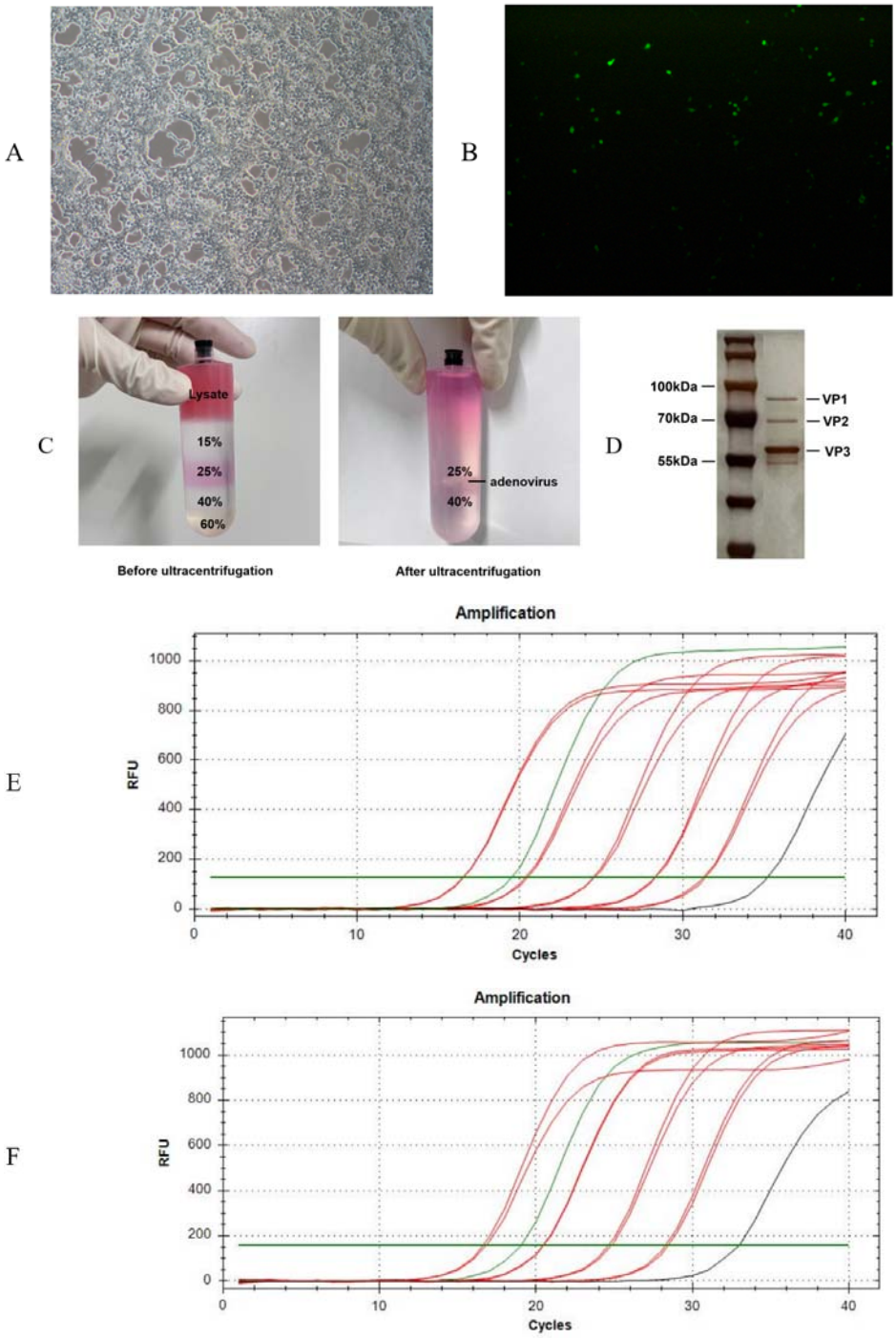


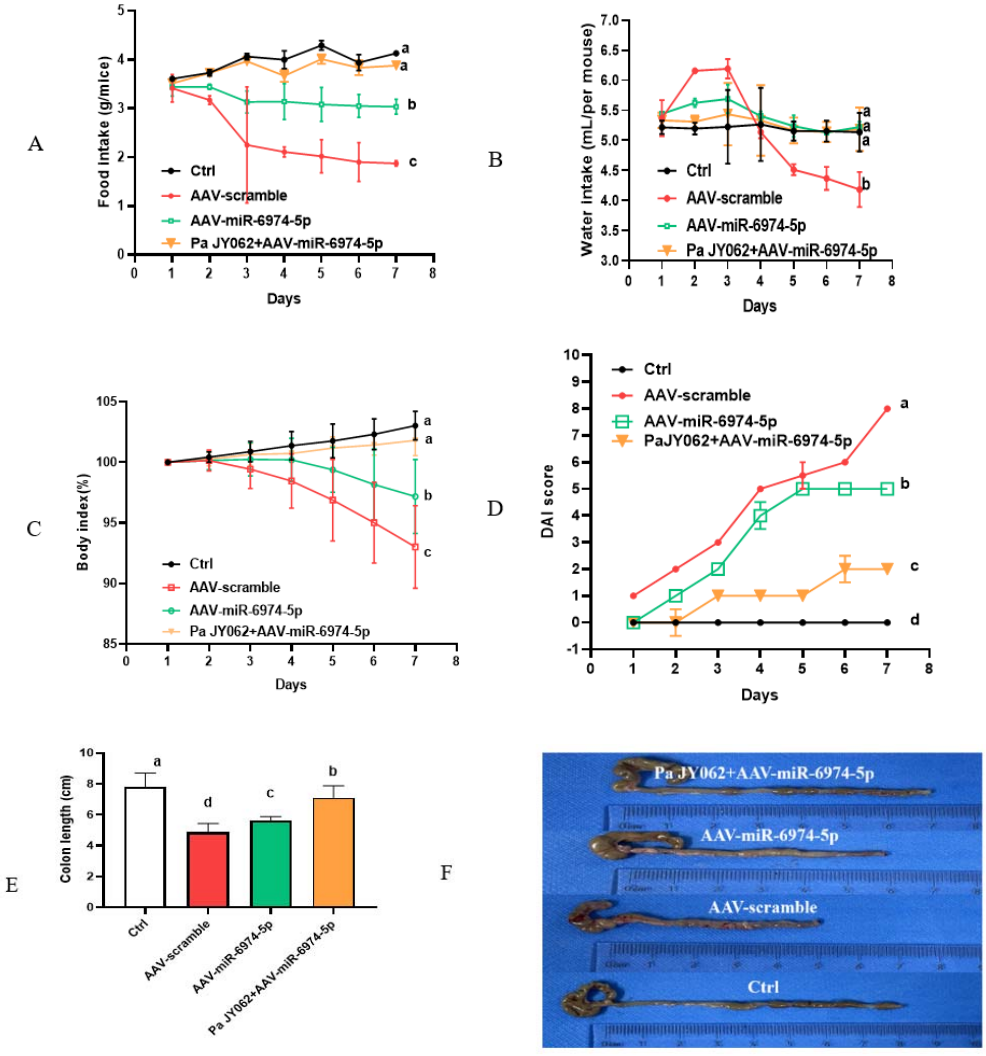
Fig.5. Successful construction and validation of the recombinant pAV-CD68-GFP-miR30-shRNA-miRNA-6974-5p vector. **(A)** Cytopathic effects observed in HEK293T cells during viral packaging. **(B)** GFP fluorescence confirming successful transduction and expression of the recombinant vector. **(C)** Iodixanol density gradient centrifugation for AAV purification. **(D)** SDS-PAGE silver staining demonstrating high purity of AAV viral particles (VP1–VP3). **(E–F)** qPCR amplification curves for quantification of **(E)** AAV-miR-6974-5p and **(F)** AAV-scramble control viral genomes.

Viral particles were harvested from both culture supernatants and cell lysates, followed by purification using iodixanol density gradient centrifugation. A distinct band at the expected density confirmed effective AAV enrichment (Fig. 5C). SDS-PAGE silver staining revealed clear VP1–VP3 capsid protein bands with minimal degradation, indicating high purity (Fig. 5D).

Viral titers were determined by qPCR, showing specific amplification curves (Fig. 5E-F). The final titer of pAV-CD68-GFP-miR30-shRNA-miRNA-6974-5p was 5.05×10^{13} vg/mL, and the scramble control was 7.27×10^{13} vg/mL, both suitable for in vivo applications. These results demonstrated the successful production of high-titer, pure pAV-CD68-GFP-miR30-shRNA-miRNA-6974-5p vectors.

3.11 AAV2-miR-6974-5p ameliorated clinical symptoms

To investigate whether miR-6974-5p contributes to the mitigation of DSS-induced colitis, we employed an AAV-mediated delivery system to overexpress this miRNA in vivo. DSS-treated AAV2-miR-scramble mice exhibited typical colitis manifestations, including reduced food intake, an initial increase followed by a decline in water consumption, significant body weight loss, elevated DAI scores, and colon shortening (Fig. 6A-F, $P < 0.05$). In contrast, mice receiving AAV2-miR-6974-5p showed significant amelioration of these parameters ($P < 0.05$). Moreover, combined treatment with AAV2-miR-6974-5p and Pa JY062 further enhanced these protective effects compared to AAV2-miR-6974-5p alone ($P < 0.05$), supporting that miR-6974-5p acts as a key downstream mediator of Pa JY062's anti-inflammatory action.



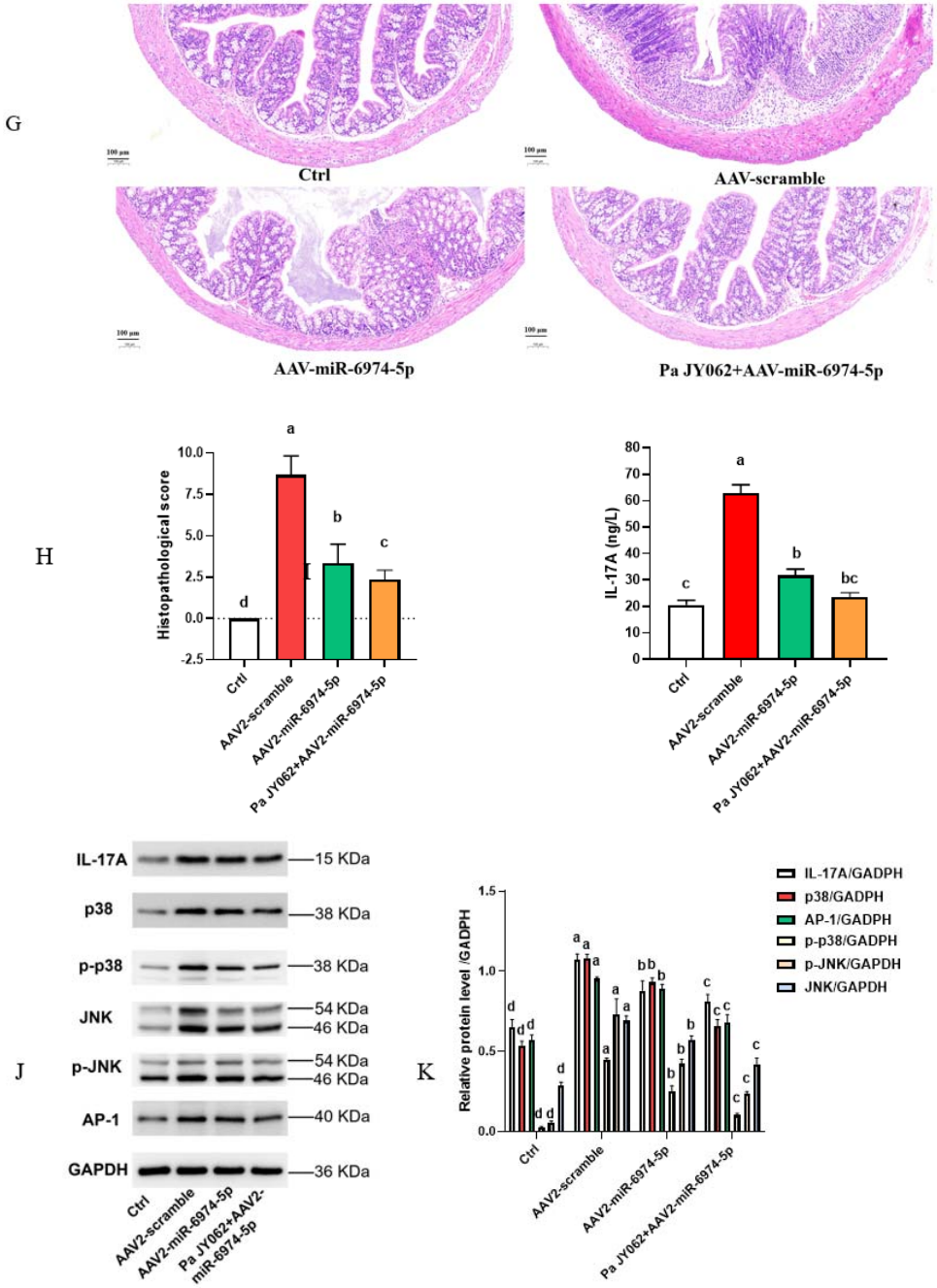


Fig.6. In vivo relieve effects of AAV-mediated miR-6974-5p overexpression in DSS-induced colitis. **(A)** Food intake, **(B)** water consumption, **(C)** body weight change, and **(D)** disease activity index (DAI) score during the experimental period. **(E)** Quantification of colon length and **(F)** representative macroscopic colon images. **(G)** Representative H&E-stained colon sections and **(H)** corresponding histopathological scores**. (I)** Colonic IL-17A levels measured by ELISA. **(J)** Western blot analysis of IL-17A, p38,p-p38,JNK,p-JNK and AP-1 protein expression, with **(K)** corresponding densitometric quantification. GAPDH served as the loading control. AAV2-miR-6974-5p: mice receiving pAV-CD68-GFP-miR30-shRNA-miRNA-6974-5p vector; Pa JY062 + AAV2-miR-6974-5p: mice receiving combined treatment with AAV2-miR-6974-5p and Pa JY062 (800 mg/kg); AAV2-miR-scramble: mice receiving pAV-CD68-GFP-miR30-shRNA-miR-scramble vector control AAV. Data are presented as mean ± SEM (n = 3).

3.12 AAV2-miR-6974-5p ameliorated colonic histopathology

H&E staining revealed significant histopathological differences among the groups. Colons from the Ctrl group showed an intact intestinal epithelium with regularly arranged crypts. In contrast, the AAV2-scramble group showed severe pathological alterations in the colon, including ulceration of the intestinal epithelium, crypt loss, and transmural inflammatory cell infiltration. AAV2-miR-6974-5p treatment significantly ameliorated these pathological features,

manifesting as preserved mucosal integrity, reduced crypt loss, and attenuated inflammation, demonstrating its protective effect against colonic injury. Notably, the combined treatment with AAV2-miR-6974-5p and Pa JY062 resulted in the most pronounced protection, with nearly intact mucosal architecture, minimal inflammatory infiltration, and the lowest histopathological scores (Fig. 6G-H, $P < 0.05$). These results further support that Pa JY062 acts by upregulating miR-6974-5p, thereby alleviating colonic injury through enhanced mucosal protection and reduced inflammation.

3.13 miR-6974-5p regulated IL-17A secretion in colonic tissues

To determine the effect of miR-6974-5p on systemic IL-17A-mediated inflammation, colonic IL-17A levels were quantified by ELISA in Ctrl, AAV2-scramble, and AAV2-miR-6974-5p treated mice. As shown in Fig. 6I, the colon IL-17A levels in the AAV2-scramble group were significantly higher than those in the control group (62.78±3.26 ng/L vs. 20.58±1.73 ng/L, $P < 0.05$), indicating a stronger pro-inflammatory state. In contrast, the colon IL-17A levels in the AAV2-miR-6974-5p group were significantly reduced (31.76±2.34 ng/L), showing a 49.41% decrease compared to the AAV2-scramble group ($P < 0.05$). Consistent with the phenotypic improvements, colonic IL-17A levels in the Pa JY062+AAV2-miR-6974-5p group were further reduced (23.64 ± 1.54 ng/L) compared to the AAV2-miR-6974-5p group (31.76±2.34 ng/L), reaching levels comparable to the control group ($P > 0.05$, Fig. 6I). This demonstrates that miR-6974-5p alleviates systemic inflammatory responses by inhibiting IL-17A, and that Pa JY062 can exert the same effect as overexpressing miR-6974-5p by regulating this miRNA to inhibit colitis development.

3.14 miR-6974-5p attenuated colitis by suppressing the IL-17A/MAPK/AP-1 signaling axis

Preliminary transcriptome sequencing revealed that IL-17A, a target of miR-6974-5p, together with its downstream signaling molecules, including p38, p-p38, JNK, p-JNK and AP-1, are key altered pathways closely associated with murine colitis. The experimental results showed that compared with the Ctrl group, the protein expression levels of IL-17A, p38, p-p38, JNK, p-JNK and AP-1 were significantly upregulated in the AAV2-scramble group (disease model group), confirming the activation of the IL-17 signaling pathway in colitis. AAV2-miR-6974-5p intervention significantly inhibited the expression of these proteins, and the combined treatment with AAV2-miR-6974-5p and Pa JY062 achieved the most pronounced suppression (Fig. 6J-K). These results indicate that miR-6974-5p exerts anti-inflammatory effects by targeting IL-17A and its downstream MAPK/AP-1 signaling axis, and that Pa JY062 acts through upregulating this miRNA to alleviate colitis.

4. Discussion

The complex pathogenesis of UC is partly driven by dysregulated miRNA-mRNA interactions. This study identified the miR-6974-5p/IL-17A axis as a crucial regulatory relationship through which a high-dose postbiotic (HP) alleviates DSS-induced colitis. We demonstrated that miR-6974-5p serves as a pivotal regulator, mitigating intestinal inflammation by directly targeting IL-17A and suppressing its downstream MAPK/AP-1 signaling. This finding was consistent with the recognized role of IL-17A as a master regulator in UC pathogenesis, driving inflammatory responses and tissue damage [14, 15]. However, while the pro-inflammatory function of IL-17A was well-established, the endogenous mechanisms that fine-tune its expression, particularly through postbiotic-mediated miRNA regulation, remain poorly understood. Our work bridged this gap by not only identifying miR-6974-5p as a novel upstream suppressor of IL-17A but also by elucidating a

complete signaling pathway from microbial intervention to inflammatory resolution. This provided a mechanistic explanation for the anti-inflammatory effects of postbiotics that extended beyond previous observational studies.

The DSS-induced colitis model was a well-established experimental system that recapitulates key features of human UC, including epithelial barrier disruption, robust innate immune activation, and a cytokine profile dominated by IL-17A and other pro-inflammatory mediators [16, 17]. Pa JY062 is a novel dairy-derived postbiotic that significantly alleviated intestinal inflammation, restored disrupted intestinal barrier function, and modulated gut microbiota imbalance in vitro and in vivo [11, 12]. miRNAs have emerged as pivotal multi-target regulators capable of simultaneously modulating intestinal barrier integrity, immune responses, and microbial homeostasis, thereby playing a central role in UC pathogenesis [18]. However, the mechanism by which Pa JY062 influenced the miRNA-mRNA regulatory network remained entirely unexplored. To bridge this critical knowledge gap, we employed transcriptomic approach to systematically analysis the miRNA and mRNA expression changes in the colon, aiming to identify the key regulatory axis through which Pa JY062 exerts its relief effects.

Our transcriptomic screening identified 14 miRNAs modulated by Pa JY062, among which miR-146b-5p, miR-155-5p, miR-135b-5p, and miR-6974-5p exhibited the most consistent dysregulation across treatment groups, suggesting their potential role in the alleviative response (Table 5). Notably, our findings align with established human UC pathology. Both miR-146b-5p and miR-155-5p showed elevated expression in UC patient serum [19, 20], with miR-155-5p known to exacerbate inflammation through *SOCS1* targeting and *FOXO3a* suppression [21]. Similarly, upregulated miR-135b-5p in both UC colon (Inciuraite et al., 2024), appeared to promote inflammatory responses, while miR-375-3p was significantly downregulated in active UC patients [22] where its target *IRF7* promoted ferroptosis via *SLC11A2* transcription [23]. The elevated serum levels of miR-106a-5p in UC patients [24] and its role in limiting Treg-mediated IL-10 production [22] further supports the relevance of our screening approach.

It is noteworthy that the functional impact of several miRNAs appears to be context-dependent. While miR-142a-3p exhibited protective effects in our system (Table 5), previous reports indicated it promotes *Limosilactobacillus reuteri* growth to alleviate colitis [25], suggesting strain-specific effects in gut immunity. Similarly, miR-31-5p upregulation in UC correlated with AMPK downregulation, and its inhibition promoted M2 macrophage polarization to ameliorate colitis [26]. miR-142-5p, elevated in UC patient mucosa, suppressed TNF-α-induced inflammatory cytokine production [27], supporting its protective role. Most significantly, we identified four novel miRNAs, miR-6974-5p, miR-6538, miR-7094-1-5p, and miR-7013-3p, with no prior reported function in colitis, representing promising candidates for future mechanistic investigation into Pa JY062's relieved actions.

Understanding miRNA function requires the identification of their target genes, as miRNAs exert their biological effects not directly but through the specific binding and regulation of downstream targets [28]. Bioinformatic prediction revealed that these miRNAs target key immune regulators, forming a coordinated network (Table 6). miR-155-5p was predicted to target *Icos*, *Il6ra*, and *Cebpb*, these genes critical for T cell activation and macrophage polarization [29-31]. Similarly, miR-146b-5p was predicted to modulate the MAPK pathway and macrophage polarization through targets like *Braf* and *Klf4*, extended its known function beyond innate immune feedback [32, 33]. Notably, novel miRNAs including

miR-6974-5p and miR-7094-1-5p were predicted to target *Il17a*, while miR-7013-3p was linked to *Ccl19* (Table 6), suggesting their potential roles in previously unexplored regulatory axes.

To establish the functional context of these miRNA changes, we performed parallel mRNA transcriptome analysis. Notably, direct DSS vs HP comparison identified 622 HP-responsive genes (Fig. 1B), whose functions were predominantly GO, KEGG and Reactome enriched in immune-related processes (Fig. 2A-C). This immunomodulatory signature aligns with previous transcriptomic studies of IBD interventions [34] and confirms that immune regulation represents the core mechanism through which Pa JY062 alleviates UC. These genes were enriched in inflammatory pathways including "cytokine-cytokine receptor interaction" and "chemokine signaling pathway" (Fig. 2D), containing key pro-inflammatory mediators in UC such as *Il1a*, *Il6*, *Il17a*, *Tnf*, *Ccl2* and *Ccl19* [35, 36].

Integration of miRNA and mRNA datasets yielded functionally coherent regulatory pairs, most notably the inverse correlation between miR-6974-5p/miR-7094-1-5p and *Il17a*, and between miR-7013-3p and *Ccl19* (Table 8). The consistent anti-correlation across groups between miRNA and their target genes mRNA [37], Pa JY062 restored miRNA expression to suppress pivotal inflammatory mediators. This coordinated action involves the inhibition of *IL-17A*, a master driver of inflammation and barrier damage [38], alongside *CCL19*, a key chemokine governing lymphocyte homing [39]. This placed the miR-6974-5p/miR-7094-1-5p/IL-17A and miR-7013-3p/CCL19 axes at the potential heart of the Pa JY062 mechanism, through which it concurrently restrained pro-inflammatory signaling and leukocyte recruitment to alleviate colitis.

RAW264.7 cells, a well-established macrophage cell line, produce IL-17A in response to LPS treatment [40-42]. Hence, further in vitro functional assays established the central role of miR-6974-5p within the Pa JY062-mediated regulatory network (Fig. 4). Transfection with miR-6974-5p mimics significantly suppressed IL-17A expression at the mRNA, protein, and secretory levels in RAW264.7 cells, whereas inhibition of endogenous miR-6974-5p markedly enhanced IL-17A production (Fig. 4A-G). In contrast, parallel experiments with miR-7094-1-5p and miR-7013-3p did not demonstrate comparable regulatory effects. The mechanism of miR-6974-5p involved the fine-tuning of a pivotal cytokine, which aligns with established paradigms of miRNA function in disease pathogenesis, even though this specific miRNA has not been previously implicated in UC. For instance, inhibition of miR-23a and miR-155 had been shown to mitigate neutrophil-mediated tissue damage and enhance mucosal healing [43]. Genetic ablation of miR-21 conferred resistance to DSS-induced colitis [44], and miR-145 had been identified as a fibroblast-specific miRNA associated with tissue repair in IBD [45]. These findings collectively outlined a complex network of miRNA-mediated regulation in intestinal inflammation. Our study introduced a critical new node into this network: miR-6974-5p, which exerted a protective effect in colitis by directly targeting and suppressing the master pro-inflammatory cytokine IL-17A.

The dual-luciferase reporter assay served as a direct method for validating such miRNA-target interactions [46]. This approach had been effectively applied in IBD research, to demonstrate that miR-330 suppressed IRAK1 expression to alleviate DSS-induced colonic injury [47]. In line with these findings, we confirmed that overexpression of miR-6974-5p significantly suppressed the luciferase activity of a wild-type IL-17A 3'UTR reporter, an effect that was completely abolished upon mutation of the predicted binding site (Fig. 4H-I). This provides direct evidence that miR-6974-5p binds specifically to the IL-17A 3'UTR via its seed sequence to mediate post-transcriptional repression.

To establish the therapeutic relevance of miR-6974-5p in vivo, we developed a recombinant vector that enabled targeted miRNA overexpression in mice [48]. This system utilizes endogenous miRNA processing machinery to generate functional miR-6974-5p, which subsequently silences IL-17A expression through RNA interference. Our data demonstrated that miR-6974-5p overexpression (AAV2-miR-6974-5p) by pAV-CD68-GFP-miR30-shRNA-miRNA-6974-5p vector significantly alleviated DSS-induced colitis symptoms. Consistent with previous studies on miRNA regulation of mRNA expression [49-51], mice treated with AAV2-miR-6974-5p showed improved nutritional intake, reduced weight loss and colon shortening, and lower disease activity scores (Fig. 6A-H). Notably, the combined treatment with Pa JY062 and AAV-mediated miR-6974-5p overexpression produced enhanced protective effects compared to either intervention alone, providing key evidence that miR-6974-5p functions as a critical downstream effector of Pa JY062. These improvements correlated with suppressed IL-17A-mediated inflammation (Fig. 6I), consistent with our in vitro findings. This aligns with previous reports that miRNA-based interventions can ameliorate colitis by regulating IL-17A pathways and Th1/Th17 immune responses [52]. Mechanistic investigation revealed that IL-17A functions as a key regulator in IL-17 pathway and activated downstream MAPK/AP-1 signaling. Through inhibiting IL-17A production, miR-6974-5p attenuated IL-17 receptor signaling, reduced MAPK phosphorylation (p-p38, p-JNK), and suppressed AP-1 activation (Fig. 6J-K). This cascade ultimately decreased pro-inflammatory cytokine expression and immune cell infiltration, leading to tissue repair.

A key strength of this study lies in the systematic progression from high-throughput transcriptomic screening to comprehensive functional validation, which encompassed in vitro gain- and loss-of-function experiments, direct binding confirmation via dual-luciferase assay, and in vivo therapeutic assessment using a targeted AAV delivery system. This multi-layered approach robustly established the miR-6974-5p/IL-17A/MAPK axis as a novel mechanism for the postbiotic Pa JY062. Furthermore, the discovery of previously uncharacterized miRNAs provided valuable resources for future research into IBD pathogenesis.

Several limitations of this study should be noted. First, a formal loss-of-function experiment (e.g., inhibiting miR-6974-5p during Pa JY062 treatment) was not performed, which would provide direct evidence for the necessity of this miRNA in mediating Pa JY062's effects. Second, the cellular origin of the miR-6974-5p/IL-17A axis remains unclear. Our AAV vector utilized the CD68 promoter, which primarily targets macrophages, suggesting that miR-6974-5p expression in these cells may be crucial for its anti-inflammatory effects. However, IL-17A is mainly produced by Th17 cells, γδ T cells, ILC3s and other cell types, while RAW264.7 and other macrophages are not the classical source of IL-17A. Whether the regulatory interaction between miR-6974-5p and IL-17A occurs in macrophages, T cells, or both, and how this cell-specific regulation contributes to the overall protective effect, warrants further investigation using cell type-specific knockout models or single-cell approaches. Third, the causal sequence of the miR-6974-5p/IL-17A/MAPK/AP-1 axis has not been fully delineated. While our data demonstrate that miR-6974-5p directly targets IL-17A, it remains possible that the observed changes in p38, p-p38, JNK, p-JNK and AP-1 are, at least in part, secondary consequences of reduced IL-17A-driven inflammation rather than direct effects of miR-6974-5p. Future studies using IL-17A neutralizing antibodies in combination with miR-6974-5p manipulation could help disentangle direct from indirect effects. Fourth, the AAV validation experiment lacked a DSS + PaJY062 alone group, which limits formal evaluation of whether the enhanced effect of combined treatment is additive or synergistic. Future investigations using cell type-specific knockout models, organoid-based coculture systems,

or clinical trials will be necessary to address these questions and to evaluate the translational potential of Pa JY062 and miR-6974-5p as therapeutic targets in UC. In addition, future studies incorporating a DSS + PaJY062 alone group are needed to formally evaluate the nature of the interaction between PaJY062 and miR-6974-5p.

5. Conclusion

In conclusion, this study demonstrates that the dairy-derived postbiotic Pa JY062 alleviates DSS-induced colitis in mice by upregulating miR-6974-5p, which directly targets IL-17A and suppresses the downstream MAPK/AP-1 signaling pathway. The enhanced protective effect of combined treatment with Pa JY062 and miR-6974-5p overexpression further supports that this miRNA acts as a key downstream mediator of Pa JY062. These findings contribute to our understanding of the connection between food-derived interventions and host molecular responses, providing a robust scientific foundation for developing Pa JY062-based functional foods or adjunctive therapies for UC management.

Acknowledgements

This research received financial backing from the Heilongjiang Provincial Natural Science Foundation Project (LH2023C033).

Ethics statement

The animal study protocol was approved by the Animal Ethics Committee of Northeast Agricultural University (approval number: NEAUEC20230422), ensuring strict observance of animal welfare and ethical standards.

Conflicts of interest

The authors declare no conflicts of interest.

References

[1] X. Qin, L. Xiao, N. Li, et al., Tetrahedral framework nucleic acids-based delivery of microRNA-155 inhibits choroidal neovascularization by regulating the polarization of macrophages, Bioactive materials. 14 (2022) 134-144. https://doi.org/10.1016/j.bioactmat.2021.11.031.

[2] H.Y. Li, Z.H. You, L. Wang, et al., DF-MDA: An effective diffusion-based computational model for predicting miRNA-disease association, Molecular therapy : the journal of the American Society of Gene Therapy. 29 (2021) 1501-1511. https://doi.org/10.1016/j.ymthe.2021.01.003.

[3] A. Soroosh, K. Fang, J.M. Hoffman, et al., Loss of miR-24-3p promotes epithelial cell apoptosis and impairs the recovery from intestinal inflammation, Cell Death Dis. 13 (2021) 8. https://doi.org/10.1038/s41419-021-04463-4.

[4] É. Boros, Z. Hegedűs, Z. Kellermayer, et al., Global alteration of colonic microRNAome landscape associated with inflammatory bowel disease, Front Immunol. 13 (2022) 991346. https://doi.org/10.3389/fimmu.2022.991346.

[5] Q. Shen, Z. Huang, L. Ma, et al., Extracellular vesicle miRNAs promote the intestinal microenvironment by interacting with microbes in colitis, Gut Microbes. 14 (2022) 2128604. https://doi.org/10.1080/19490976.2022.2128604.

[6] S. Salminen, M.C. Collado, A. Endo, et al., The International Scientific Association of Probiotics and Prebiotics (ISAPP) consensus statement on the definition and scope of postbiotics, Nature Reviews Gastroenterology & Hepatology. 18 (2021) 649-667.

[7] Y. Chen, J. Huang, R. Chen, et al., Sustained release of dermal papilla-derived extracellular vesicles from injectable microgel promotes hair growth, Theranostics. 10 (2020) 1454-1478. https://doi.org/10.7150/thno.39566.

[8] J. Xie, Q. Li, S. Nie, Bacterial extracellular vesicles: An emerging postbiotic, Trends in Food Science & Technology. 143 (2024) 104275. https://doi.org/https://doi.org/10.1016/j.tifs.2023.104275.

[9] Q. Chen, Z. Fang, Z. Yang, et al., *Lactobacillus plantarum*-Derived Extracellular Vesicles Modulate Macrophage Polarization and Gut Homeostasis for Alleviating Ulcerative Colitis, Journal of Agricultural and Food Chemistry. 72 (2024) 14713-14726. https://doi.org/10.1021/acs.jafc.4c01758.

[10] X. Nie, Q. Li, H. Ji, et al., *Bifidobacterium longum* NSP001-derived extracellular vesicles ameliorate ulcerative colitis by modulating T cell responses in gut microbiota-(in)dependent manners, NPJ Biofilms Microbiomes. 11 (2025) 27. https://doi.org/10.1038/s41522-025-00663-4.

[11] J. Guo, Y. Zhao, W. Guo, et al., Effects of *Lactobacillus paracasei* JY062 Postbiotic on Intestinal Barrier, Immunity, and Gut Microbiota, Nutrients. 17 (2025) https://doi.org/10.3390/nu17071272.

[12] J. Guo, Y. Sun, K. Gao, et al., JY062 Postbiotic Alleviated 3% DSS-Induced Colitis in Mice via Integrated Antioxidant, Barrier Repair, Immunomodulatory and Microbiota Modulation, Antioxidants. 14 (2025) 1256. https://www.mdpi.com/2076-3921/14/10/1256

[13] A. Ding, X. Tang, D. Yang, et al., ERF4 and MYB52 transcription factors play antagonistic roles in regulating homogalacturonan de-methylesterification in Arabidopsis seed coat mucilage, The Plant cell. 33 (2021) 381-403. https://doi.org/10.1093/plcell/koaa031.

[14] M.A. Busch, B. Gröndahl, R.L. Knoll, et al., Patterns of mucosal inflammation in pediatric inflammatory bowel disease: striking overexpression of IL-17A in children with ulcerative colitis, Pediatric Research. 87 (2020) 839-846. https://doi.org/10.1038/s41390-019-0486-5.

[15] C.S. Howe, M. Chulkina, R. Syrcle, et al., MK2 Inhibition in CD4+ T Cells Protects Against IFNγ and IL-17A, Chronic Inflammation, and Fibrosis in Inflammatory Bowel Disease Models, Inflammatory Bowel Diseases. 31 (2025) 1664-1676. https://doi.org/10.1093/ibd/izaf026.

[16] X. Yan, C. Yang, M. Yang, et al., All-in-one theranostic nano-platform based on polymer nanoparticles for BRET/FRET-initiated bioluminescence imaging and synergistically anti-inflammatory therapy for ulcerative colitis, J Nanobiotechnology. 20 (2022) 99. https://doi.org/10.1186/s12951-022-01299-8.

[17] X. Feng, Y. Xiao, J. He, et al., Long noncoding RNA Gm31629 protects against mucosal damage in experimental colitis via YB-1/E2F pathway, JCI insight. 7 (2022) https://doi.org/10.1172/jci.insight.150091.

[18] S. Dhuppar, G. Murugaiyan, miRNA effects on gut homeostasis: therapeutic implications for inflammatory bowel disease, Trends in Immunology. 43 (2022) 917-931. https://doi.org/10.1016/j.it.2022.09.003.

[19] S. Pathak, A.R. Grillo, M. Scarpa, et al., MiR-155 modulates the inflammatory phenotype of intestinal myofibroblasts by targeting SOCS1 in ulcerative colitis, Exp Mol Med. 47 (2015) e164. https://doi.org/10.1038/emm.2015.21.

[20] D.M.A. Elzoghby, N.H. Mahmoud, A.S. Allam, et al., Serum miRNA 146b-5p a pharmacodynamic biomarker in adult inflammatory bowel disease, The Egyptian journal of immunology. 32 (2025) 40-47. https://doi.org/10.55133/eji.320305.

[21] J. Cheng, Y. Zhang, J. Yang, et al., MiR-155-5p modulates inflammatory phenotype of activated oral lichen-planus-associated-fibroblasts by targeting SOCS1, Molecular biology reports. 49 (2022) 7783-7792. https://doi.org/10.1007/s11033-022-07603-x.

[22] R. Yarani, A. Shojaeian, O. Palasca, et al., Differentially Expressed miRNAs in Ulcerative Colitis and Crohn's Disease, Frontiers in Immunology. Volume 13 - 2022 (2022) https://doi.org/10.3389/fimmu.2022.865777.

[23] Z. Chen, Q. Gu, R. Chen, Promotive role of IRF7 in ferroptosis of colonic epithelial cells in ulcerative colitis by the miR-375-3p/SLC11A2 axis, Biomolecules & biomedicine. 23 (2023) 437-449. https://doi.org/10.17305/bjbms.2022.8081.

[24] D. Li, L. Liu, X. Du, et al., MiRNA-374b-5p and miRNA-106a-5p are related to inflammatory bowel disease via regulating IL-10 and STAT3 signaling pathways, BMC gastroenterology. 22 (2022) 492. https://doi.org/10.1186/s12876-022-02533-1.

[25] L. He, X. Zhou, Y. Liu, et al., Fecal miR-142a-3p from dextran sulfate sodium-challenge recovered mice prevents colitis by promoting the growth of *Lactobacillus reuteri*, Molecular therapy : the journal of the American Society of Gene Therapy. 30 (2022) 388-399. https://doi.org/10.1016/j.ymthe.2021.08.025.

[26] Y. Yuan, S. Deng, J. Yang, et al., Antagomir of miR-31-5p modulates macrophage polarization via the AMPK/SIRT1/NLRP3 signaling pathway to protect against DSS-induced colitis in mice, Aging (Albany NY). 16 (2024) 5336-5353. https://doi.org/10.18632/aging.205651.

[27] J. Han, Y. Li, B. Zhang, et al., lncRNA TUG1 regulates ulcerative colitis through miR-142-5p/SOCS1 axis, Microbial Pathogenesis. 143 (2020) 104139. https://doi.org/https://doi.org/10.1016/j.micpath.2020.104139.

[28] M. Pu, J. Chen, Z. Tao, et al., Regulatory network of miRNA on its target: coordination between transcriptional and post-transcriptional regulation of gene expression, Cellular and Molecular Life Sciences. 76 (2019) 441-451. https://doi.org/10.1007/s00018-018-2940-7.

[29] F. Piattini, N.D. Sidiropoulos, I. Berest, et al., IL-6 mediates defense against influenza virus by promoting protective antibody responses but not innate inflammation, Mucosal Immunology. 18 (2025) 596-606. https://doi.org/https://doi.org/10.1016/j.mucimm.2025.02.001.

[30] M. Mammadli, R. Harris, L. Suo, et al., Interleukin-2-inducible T-cell kinase (Itk) signaling regulates potent noncanonical regulatory T cells, Clinical and translational medicine. 11 (2021) e625. https://doi.org/10.1002/ctm2.625.

[31] L. Zhao, F. Lv, Y. Zheng, et al., Characterization of an Aging-Based Diagnostic Gene Signature and Molecular Subtypes With Diverse Immune Infiltrations in Atherosclerosis, Frontiers in molecular biosciences. 8 (2021) 792540. https://doi.org/10.3389/fmolb.2021.792540.

[32] C. Liu, F. Hu, G. Jiao, et al., Dental pulp stem cell-derived exosomes suppress M1 macrophage polarization through the ROS-MAPK-NFκB P65 signaling pathway after spinal cord injury, J Nanobiotechnology. 20 (2022) 65. https://doi.org/10.1186/s12951-022-01273-4.

[33] D.L. Ou, C.W. Chen, C.L. Hsu, et al., Regorafenib enhances antitumor immunity via inhibition of p38 kinase/Creb1/Klf4 axis in tumor-associated macrophages, Journal for immunotherapy of cancer. 9 (2021) https://doi.org/10.1136/jitc-2020-001657.

[34] Y. Yuan, H. Hu, Z. Sun, et al., Combining Metagenomics, Network Pharmacology and RNA-Seq Strategies to Reveal the Therapeutic Effects and Mechanisms of Qingchang Wenzhong Decoction on Inflammatory Bowel Disease in Mice, "Drug Design, Development and Therapy". 18 (2024) 4273-4289. https://doi.org/10.2147/DDDT.S473688.

[35] Y.J. Shi, S.J. Hu, Q.Q. Zhao, et al., Toll-like receptor 4 (TLR4) deficiency aggravates dextran sulfate sodium (DSS)-induced intestinal injury by down-regulating IL6, CCL2 and CSF3, Annals of translational medicine. 7 (2019) 713. https://doi.org/10.21037/atm.2019.12.28.

[36] Y. Su, Z. Cui, C. Chen, et al., *Lactobacillus paracasei* JY062 with its exopolysaccharide ameliorates intestinal inflammation on DSS-induced experimental colitis through TLR4/MyD88/NF-κB signaling pathway, Food Bioscience. 63 (2025) 105689. https://doi.org/https://doi.org/10.1016/j.fbio.2024.105689.

[37] I. Simeone, C. Rubolino, Teresa Maria R. Noviello, et al., Prediction and pan-cancer analysis of mammalian transcripts involved in target directed miRNA degradation, Nucleic Acids Research. 50 (2022) 2019-2035. https://doi.org/10.1093/nar/gkac057.

[38] L. N, M. P, L. Y, et al., Gut microbiota-derived 12-ketolithocholic acid suppresses the IL-17A secretion from colonic group 3 innate lymphoid cells to prevent the acute exacerbation of ulcerative colitis, Gut microbes. 15 (2023) 2290315. https://doi.org/10.1080/19490976.2023.2290315.

[39] G.L. Moschovakis, A. Bubke, M. Friedrichsen, et al., The chemokine receptor CCR7 is a promising target for rheumatoid arthritis therapy, Cellular & molecular immunology. 16 (2019) 791-799. https://doi.org/10.1038/s41423-018-0056-5.

[40] H. Wang, R. Li, Y. Rao, et al., Enhancement of the Bioavailability and Anti-Inflammatory Activity of Glycyrrhetinic Acid via Novel Soluplus®—A Glycyrrhetinic Acid Solid Dispersion, Pharmaceutics. 14 (2022) 1797. https://www.mdpi.com/1999-4923/14/9/1797

[41] S. Ye, J. Liu, S. Huang, et al., Coated nanoparticles enhance immune efficacy of Helicobacter pylori outer membrane vesicles by activating Th1/Th2/Th17 responses, The Journal of Pharmacology and Experimental Therapeutics. 392 (2025) 103669. https://doi.org/https://doi.org/10.1016/j.jpet.2025.103669.

[42] W. Fu, Z. Huang, W. Li, et al., Copper–luteolin nanocomplexes for Mediating multifaceted regulation of oxidative stress, intestinal barrier, and gut microbiota in inflammatory bowel disease, Bioactive Materials. 46 (2025) 118-133. https://doi.org/https://doi.org/10.1016/j.bioactmat.2024.12.004.

[43] V. Butin-Israeli, T.M. Bui, H.L. Wiesolek, et al., Neutrophil-induced genomic instability impedes resolution of inflammation and wound healing, J Clin Invest. 129 (2019) 712-726. https://doi.org/10.1172/jci122085.

[44] D.G.W. Johnston, M.A. Williams, C.A. Thaiss, et al., Loss of MicroRNA-21 Influences the Gut Microbiota, Causing Reduced Susceptibility in a Murine Model of Colitis, J Crohns Colitis. 12 (2018) 835-848. https://doi.org/10.1093/ecco-jcc/jjy038.

[45] L. Y, W. Y, C. S, et al., The landscape of miRNA-mRNA regulatory network and cellular sources in inflammatory bowel diseases: insights from text mining and single cell RNA sequencing analysis, Frontiers in immunology. 15 (2024) 1454532. https://doi.org/10.3389/fimmu.2024.1454532.

[46] F. Kern, L. Krammes, K. Danz, et al., Validation of human microRNA target pathways enables evaluation of target prediction tools, Nucleic Acids Research. 49 (2020) 127-144. https://doi.org/10.1093/nar/gkaa1161.

[47] Q. Zhang, S.F. Wang, miR-330 alleviates dextran sodium sulfate-induced ulcerative colitis through targeting IRAK1 in rats, The Kaohsiung journal of medical sciences. 37 (2021) 497-504. https://doi.org/10.1002/kjm2.12359.

[48] I. Kraszewska, M. Tomczyk, K. Andrysiak, et al., Variability in Cardiac miRNA-122 Level Determines Therapeutic Potential of miRNA-Regulated AAV Vectors, Molecular therapy. Methods & clinical development. 17 (2020) 1190-1201. https://doi.org/10.1016/j.omtm.2020.05.006.

[49] Q. Feng, Y. Li, H. Zhang, et al., Deficiency of miRNA-149-3p shaped gut microbiota and enhanced dextran sulfate sodium-induced colitis, Molecular Therapy - Nucleic Acids. 30 (2022) 208-225. https://doi.org/https://doi.org/10.1016/j.omtn.2022.09.018.

[50] W. Zhang, X. Fu, J. Xie, et al., miR-26a attenuates colitis and colitis-associated cancer by targeting the multiple intestinal inflammatory pathways, Molecular therapy. Nucleic acids. 24 (2021) 264-273. https://doi.org/10.1016/j.omtn.2021.02.029.

[51] S. Zhao, L. Zhu, W. Feng, et al., MicroRNA-602 prevents the development of inflammatory bowel diseases in a microbiota-dependent manner, Experimental and therapeutic medicine. 22 (2021) 1373. https://doi.org/10.3892/etm.2021.10808.

[52] C. He, Y. Shi, R. Wu, et al., miR-301a promotes intestinal mucosal inflammation through induction of IL-17A and TNF-α in IBD, Gut. 65 (2016) 1938-1950. https://doi.org/10.1136/gutjnl-2015-309389.